

# Assessment of the thermodynamics efficiency of a cement vertical raw mill using Aspen Plus and artificial intelligence models

Anthony I. Okoji (✉ [anthony.okoji@covenantuniversity.edu.ng](mailto:anthony.okoji@covenantuniversity.edu.ng))

Covenant University

Ambrose N. Anozie

Obafemi Awolowo University

James A. Omoleye

Covenant University



---

## Research Article

**Keywords:** Energy efficiency, Vertical raw mill, Process simulator, Adaptive neuro-fuzzy inference systems, genetic algorithm, particle swarm optimization

**Posted Date:** June 12th, 2023

**DOI:** <https://doi.org/10.21203/rs.3.rs-3039610/v1>

**License:**   This work is licensed under a Creative Commons Attribution 4.0 International License. [Read Full License](#)

---

# Abstract

Globally, cement plants are striving to improve their energy efficiency. Therefore, it is critical for cement plant operations to increase the monitoring and control of a vertical raw mill energy process. This technology has attracted the interest of the cement industry with its proven benefits in cement grinding applications. A process simulator was used to study an industrial-scale vertical raw mill (VRM) with 65.4% energy efficiency. The paper proposes further a new model based on grid partitioning, sub-clustering, and fuzzy c-means, which incorporates genetic algorithms (GAs) and particle swarm optimizations (PSOs). VRM data from a steady plant process operation, such as raw material output, material moisture, kiln hot gas, mill fan flow, grinding pressure, and separator speed, was used as input to the prediction model. ANFIS-based prediction models are compared with process simulator predictions to determine the most accurate based on prediction performance criteria. Based on the results, the ANFIS model with sub-clustering assimilated with PSO is the most accurate prediction model for VRM energy efficiency. The coefficient of regression ( $R^2$ ) and root mean square error (RMSE) obtained by this model are 0.945 and 1.3006. The results also showed that VRM's energy efficiency decreased from 65.4 to 64.2% when the separator speed increased from 50 to 75 rpm; product particle size on P90 $\mu$ m decreased from 18.2–10.8%. Finally, the proposed ANFIS based model can be considered to be an efficient technique for predicting the energy efficiency of VRM production processes.

## 1.0. Introduction

Cement production globally is estimated at 4.2 billion tons in 2019, and cement grinding consuming approximately 2.0 percent of the total available electrical energy (Ghalandari, Majd, & Golestanian, 2019; A. I. Okoji, Anozie, Omoleye, Taiwo, & Osuolale, 2022b). Consequently, cement plants consume an average of 100 kWh per ton of cement produced, with two-thirds of these kWh utilized by raw material and cement mills (Tsakalakis & Stamboltzis, 2008). Vertical raw mill processes have become a high priority for all stakeholders in the cement industry because of the critical role raw mills play in cement production and the quest to make them more energy efficient. Thus, cement sustainability depends on increasing the energy efficiency through driving down on power consumption of the industry (Cai, Liu, Lai, Li, Cunha, & Hu, 2019; A. I. Okoji, Babatunde, Anozie, & Omoleye, 2018).

In a study performed by Worrell, Martin, & Price (2000), in the US cement manufacturing sector between 1970 and 1997, it was concluded that the use of blended cement would help in the drive for improved energy efficiency and carbon dioxide emission reduction (Kong, Price, Hasanbeigi, Liu, & Li, 2013). Zhang, Zhao, Lu, Ni, & Li (2017) investigated cement plant waste energy recovery, studied trass mill waste energy recovery leading to a 10 percent increased energy efficiency and a 56 percent decrease in exergy loss. Consequently, the need for more energy-efficient cement industries should consistently be the main focus worldwide. The grinding process and product quality are greatly affected by particle size, making it a very energy-intensive process in cement production (Altun, Benzer, Aydogan, & Gerold, 2017). Various techniques were employed by researchers to optimize the grinding systems for most efficient production process. A vertical roller mill (VRM) is usually controlled and optimized in order of importance related to product quality, process throughput, and utility reductions. A trade-off usually has to be made between these three variables. Optimizing VRM operations is vital to achieving both product quality and energy efficiency. It is a major tool for the process industry to make a decision based on quantitative information. Rather than huge expansion, most industries will focus on maximizing resources for maximum profitability. Consequently, a study of the impact of operational parameters on ball mill energy efficiency revealed a low particle collision energy will be a reflection of coarse particle size

observed at the mill outlet fine products (Fernandes, Halim, &Wahab, 2019; Ghalandari & Iranmanesh, 2020; Simmons, Gorby, &Terembula, 2005). Therefore, to achieve a narrow particle size distribution, applying moderate energy to particles is necessary for this type of operation over a period of use (Tsakalakis & Stamboltzis, 2008). Furthermore, the power consumption of the raw mill grinding process was reduced by 6.7 percent by using exterior hot gas, as suggested in an energy and exergy analysis of the mill by Atmaca & Kanoglu (2012). A. I. Okoji et al. (2018) also studied the appropriateness of exergy calculation using Aspen Plus Process Simulator, there was no noticeable variance in the result when compared with conventional methods. In recent studies, Ghalandari, Esmaeilpour, Payvar, & Reza (2021) evaluated the energy and exergy efficiency of a cement plant and was established that the main energy input occurs as thermal energy from the material feed, while maximum exergy contribution comes from electricity. When it comes to energy efficiency, the VRM could improve milling efficiency while saving a significant amount of energy for cement plants (SCHÄFER, 2002).

Process simulators are essential to optimizing VRM, but the complex nature of these processes has led to a number of assumptions that may limit their universality (A. I. Okoji et al., 2018). As a result, the majority of mechanistic models deviate from reality and may not provide an accurate representation of reality. These mechanistic models are also computationally intensive, making them ineffective for real-time optimization. Artificial intelligence (AI) models can be used to overcome these problems (Bao, Zhu, Du, Zhong, &Qian, 2019; Gong, Yuan, Liu, &Feng, 2019). ANN is recognized as an effective tool for the development of nonlinear and multivariable systems that rely on data-driven models (A. I. Okoji, Anozie, &Omoleye, 2022a; A. I. Okoji et al., 2022b). A neural network can be used to learn complex functional relationships between systems by analyzing input and output data. This makes them ideal for real-time optimization since their evaluation is much less computationally demanding. VRM systems often use neural networks to model product specifications as outputs (Inapakurthi, Miriyala, &Mitra, 2020; Pani & Mohanta, 2014, 2015; Wang, Jia, Huang, &Chen, 2010). Other mill types, such as ball mills, have already been investigated using energy and exergy analyses, and our results will allow other researchers to compare the thermodynamic performance of another mill type with VRM.

According to this study, artificial intelligence with optimization algorithms were used in order to model the energy efficiency of vertical raw mills. Despite this, ANFIS has been used to optimize enzyme synthesis (Kumar, Singh, Arya, Bhatti, &Sharma, 2018; Uzuner & Çekmecelioğlu, 2016), biogas production prediction (Asadi, Guo, &McPhedran, 2020), air pollutant prediction (Noori, Hoshyaripour, Ashrafi, &Araabi, 2010; Shamshirband, Hadipoor, Baghban, Mosavi, Bukor, &Várkonyi-Kóczy, 2019), raw meal process exergy efficiency(A. I. Okoji, Anozie, &Omoleye, 2021), biomass prediction using grid partitioning, sub-clustering, and fuzzy cmeans clustering algorithms (Akkaya, 2016), to predict DBP (trihalomethanes) levels in the water treatment plant (C. N. Okoji, Okoji, Ibrahim, &Obinna, 2022) and vertical raw mill product quality (Fernandes et al., 2019), however, we know of no other study that utilizes this model to predict and optimize vertical raw mill energy efficiency in cement processing plants. The focus of this work was to create different models to predict vertical raw mill energy efficiency while taking plant operating data into account in order to avoid the problems of experimental testing. A unique correlation model is presented here, as well as ANFIS-based models. The fuzzy inference system is generated using grid partitioning, sub-clustering, and fuzzy cmeans clustering algorithms. A number of model structures are built for each approach by varying their associated parameters. Furthermore, artificial intelligence methods such as PSO-ANFIS-GP, PSO-ANFIS-FCM, PSO-ANFIS-SC, PSO-ANFIS-GP, PSO-ANFIS-FCM, and PSO-ANFIS-SC were applied to determine the vertical raw mill energy efficiency regarding the plant operating data. To develop the proposed models, 1026 plant operating data was collected over a range of 2020 to 2021 of a steady

state operating data to avoid a misrepresentation of data. To the best of our knowledge, no one has used the PSO-ANFIS-GP, PSO-ANFIS-FCM, PSO-ANFIS-SC GA-ANFIS-GP, GA-ANFIS-FCM, and GA-ANFIS-SC model in this context. To demonstrate their precise capacity, the obtained results were compared to the plant audit. Furthermore, the resilience of the suggested system was tested with 2022 plant operational data to evaluate the model's precision, accuracy, and reliability.

## 2.0. Theoretical analysis and method

The vertical raw mill process was modelled in this study using ASPEN Plus V10.2 for minimising Gibbs free energy. Eq. 1 describes equilibrium at constant temperature and pressure for a system.

$$dG = \sum_{i=1}^k \mu_i n_i dn_i \quad (1)$$

The Gibbs free energy of species  $i$  is  $G$ , the number of molecules of species  $i$  is  $n_i$ , the number of chemical species in the reaction mixture is  $\mu_i$  and the chemical potential of species  $i$ . A set of  $n_i$  values must be found that result in the smallest  $G$  value. The stoichiometric approach and the non-stoichiometric approach are both possible. A stoichiometrically independent reaction system describes the former case, which is usually chosen arbitrarily from a set of possible reactions. By directly minimising the Gibbs free energy for a given species, this approach determines the equilibrium composition. Most open-source literature uses a non-stoichiometric approach [Adeniyi & Ighalo 2019]. Several advantages result from this, such as the absence of having to select the possible set of reactions, the absence of divergence during computation, and the lack of having to estimate precisely the composition of the initial equilibrium.

$$G = \sum_{i=1}^k \mu_i n_i \quad (2)$$

It is necessary to ensure that  $n_i$  is in mass balance in order to estimate the smallest value of  $G$  for  $n_i$ .

$$\sum_{i=1}^k \mu_i n_i = b_i, i = 1, \dots, M \quad (3)$$

In this equation,  $\mu_i$  determines how many gram atoms of element  $I$  are in one mol of specie  $i$ ,  $b_i$  determines how many gram atoms there are in the reaction mixture and  $M$  represents the total number of atoms in the reaction mixture. Therefore, Eq. 4 can be written as follows:

$$G = \sum_{i=1}^K n_i \Delta G_i^0 + RT \sum_{i=1}^K n_i \ln y_i + RT \sum_{i=1}^K n_i \ln P \quad (4)$$

It is the expression in which  $T$  represents temperature,  $P$  represents pressure, and  $\Delta G_i^0$  represents standard Gibbs free energy of the formation of species  $i$ .  $y_i$  represents the mole fraction of that species. The objective function is expressed in Eq. 4.

Thermodynamic predictions are obtained with the help of process simulation software like ASPEN Plus utilizing this method to minimize Gibbs free energy.

A steady-flow process is analyzed using the following equations to determine work, heat interactions, and energy efficiency.

### Mass balance

Eq. (5) depicts the mass balance of the system, expressed in terms of mass.

$$\Sigma \dot{m}_{in} = \Sigma \dot{m}_{out}$$

5

According to Bejan (2016), mass flow rate is expressed, while the subscript 'in' signifies inlet and 'out' signifies outlet.

### Energy balance

Eqs (6) and (7) can be used to express energy balance equations.

$$\Sigma E_{in} = \Sigma E_{out}$$

6

$$Q_{netin} + \Sigma \dot{m}_{in} h_{in} = W_{netin} + \Sigma \dot{m}_{out} h_{out}$$

7

The rate of (energy transfer in) is represented as  $E_{in}$ . The rate of (net heat input) is expressed as;  $Q_{netin} = Q_{in} - Q_{out}$ , while the rate of (energy transfer out) is  $E_{out}$ , and the rate of (net work output) is represented as;  $W_{netin} = W_{out} - W_{in}$ , given h, the specific enthalpy. With both kinetic and potential energy constant, we can further simplify Eq. (8) to express only enthalpy flow:

$$\Sigma \dot{m}_{in} h_{in} = \Sigma \dot{m}_{out} h_{out}$$

8

Equations (7) and (8) summarize the energy balance around the vertical raw mill

$$\Sigma E_{in} = E_{rawmaterial} + E_{combustionair} + E_{hotgasgenerator} + E_{materialmoisture} + E_{kilnhotgas}$$

9

$$\Sigma E_{out} = E_{finalproduct} + E_{rawmillexitair} + E_{steam}$$

10

Equation (7) defines the system's efficiency equation

$$\eta = \frac{\Sigma \dot{E}_{out}}{\Sigma \dot{E}_{in}} \quad (11)$$

## 2.1. Process Simulation Model of Raw Mill

A vertical raw mill plant operating at 240,000 kg per hour requires a process model containing physical property parameters. The vertical raw mill process consists of three steps: drying, grinding, and separation. An air stream transports fine particles entrapped in crushed raw materials upward in the upper part of the mill. Despite Aspen Plus being a two-phase stream, this stream is treated as a "Solid-Liquid" and "Solid-Vapour" together. As soon as the mill stream leaves, fine dust and coarse dust are separated in a screen (separator). Each is used for further processing. The product (fine dust) and gas mixtures are transported to cyclones for separation into fine dust in gas streams and to be used as the kiln as feed. While fine dust is trapped in electrostatic precipitators, clean gas is allowed to escape into the atmosphere.

It is assumed that the inlet feed is homogeneous, with different particle size distributions (PSDs) in the simulation. The vertical raw mill is modelled by three stages, and the crusher (mill) model is a continuous dry grinding operation. A classifier forms the upper part of the mill, which entrains fine material from the raw material as it is crushed/milled. No chemical reaction occurs between the feed and outlet particle streams. A fine particle size reduction operation is all that is involved as shown in Fig. 1.

This simulation model was built using Aspen Plus version 10.2 "SOLID Model" inbuilt template as the basis for simulating the vertical raw mill operation in cement manufacturing. Modeling a process relies heavily on selecting a property package that accurately replicates the various physical properties of the system. Henry's Law is being used to determine the supercritical components present in the liquid phase, while Redlich-Kwong equation of state method is used to find the properties of the vapor phase. Kent-Eisenberg method is used to solve equilibrium constants and enthalpies. In every simulation, steady-state conditions are assumed.

A new feature of Aspen Plus makes it easy to model solids anywhere in a process sheet and the model was represented as blocks in Table 1. For solids handling equipment, a variety of unit operation models are available including crushers (mills), screens (separators), cyclones, and electrostatic precipitators. A flowsheet represents the streams of material and energy using blocks as shown in Fig. 2. Physicochemical properties were incorporated into the simulation calculation using a large databank. The 'Solids Template' reports properties and components flows for various types of particles, such as liquids, solids, and vapours. MIXCIPSD represents mixed conventional solids with particle sizes distributed. Models were developed based on the following assumptions: a) There is no pressure loss, turbulent motion, or air leakage because the process is in steady state. b) As a result of the process, neither atmospheric nor pressure drop occurs. c) No heat losses through the system

These processes could lead to the development of the ASPEN Plus model:

- Stream classes and the method of property selection are described.
- An extensive database for the description of system components.
- Based on unit operations of blocks, process flow sheets are created by connecting material and energy streams. Additionally, the blocks' chemical and physical reactions affect the thermodynamic conditions.

- Describes the flowrate, the feed components, and the distribution of particle size in the feed stream.

RGIBBs assist the combustion process to provide heat for the drying process. It is not necessary to comply with the specification reaction stoichiometric rules when using RGIBBS blocks. Fine dust is separated from coarse dust in a screen (separator) after the mill, and the coarse is recycled back to the mill. The separation efficiency of the screen is determined by simulating the screen sizes of entrained fine material and determining how much of it is recycled or permitted to pass as final product. A cyclone separator is also used for further dust-laden gas separation, which respects the 90% pass on the 10 micrometer scale. The centrifugal force of a gas vortex obtained from a cyclone helps remove fine dust particles from a dust-entrapped gas stream. Before the clean air is released into the atmosphere, the entrained dust particles are separated from the gas stream using an electrostatic precipitator (ESP). Electrostatic fields generated by collecting plate electrodes can effectively remove the dust particles from gas streams when the wires are placed parallel and in between the plates as shown in Fig. 2.

Table 2 displays the simulation input settings used in Aspen Plus. On the basis of the simulation data from Aspen Plus, equations (5), (6), and (7) were used to analyze the energy of the streams at steady state. Eq. 7 was used to calculate the efficiency of a cement vertical raw mill. Each stream in Aspen Plus was constructed with temperature, pressure, enthalpy, and internal energy. At both the fundamental operational and reference stages, Aspen Plus was used to measure the energy of each stream. Eqs. (8) and (9) were used to calculate maximum energy at the network's inlet and output, whereas Eq. (11) was utilized to calculate energy efficiency.

Table 1  
Aspen Plus blocks and model representation for biomass steam gasification

Block	Model	Function
MILL	CRUSHER	Breaking solid particles in a crusher into smaller particle size distribution (PSD)
MIXER	SSPLIT	Combine feed streams/mixes all of its feed streams, then splits the resulting mixture into two
SEP	SEP	Rotation and gravitational force are used to separate gas and solid particles
RGIBBS		Methane combustion occurs when Gibbs free energy minimization is applied to all possible reactions
ESP	ESP	Solids separation from a gas stream
VSCRUB	VENTURI SCRUBBER	Separating solid particles in a screen
SCREEN	SEP	Separating solid particles in a screen

Table 2  
Equipment specifications for the production of raw meals

<b>Parameters</b>	<b>Unit</b>	
<b>Rawmilloutput</b>	<i>kg/h</i>	240,000
<b>Materialmoisture</b>	<i>kg/h</i>	48,000
<b>Kilnhotgasflow</b>	<i>Nm<sup>3</sup>/h</i>	313,473
<b>Inputdustflow</b>	<i>kg/h</i>	19.353
<b>Kilnhotgasflowtemperature</b>	<i>°C</i>	380
<b>Hotgasgeneratortemperature</b>	<i>°C</i>	760
<b>Outputmaterialtemperature</b>	<i>°C</i>	92
<b>VRMOperatingPressure</b>	<i>atm</i>	1
<b>Rawmillcycloneefficiency</b>	<i>%</i>	96
<b>Classifiedseparatorefficiency</b>	<i>%</i>	86
<b>ESP – precipitatorefficiency</b>	<i>%</i>	84

## 2.2.1 The collection and processing of data

A cement vertical raw mill process was studied in a cement plant, south west, Nigeria, and both input and output variables were collected. Data was collected for about a month from the distributed control system database every minute. The operational parameters of the cement plant for the year 2021 were analyzed and obtained from its records. Raw mill output, material moisture, kiln hot gas flow, mill fan flow, grinding pressure, and separator speed are among the operational parameters. Material inconsistency in the mill process will result in high noise in the measured field data due to dust recirculation in the gas stream, particularly for the thin raw material layer under the roller. To develop a computational intelligence model, gathered information had to be screened to determine which operational parameters were relevant and consistent. The missing data was interpolated using selected data, which was analyzed statistically. A set of operational parameters was selected with 1025 monthly data points, as shown in Table 3.



Table 3  
Plant operations parameter for ANFIS model

Unit	Parameter	No. of data	Mean	Maximum	Minimum	SD	Mode
Vertical raw mill	Raw mill output (kg/hr)	1025	220008	240000	200000	14909	200000
	Material moisture (kg/hr)	1025	75000	100000	50000	18634	50000
	Kiln hot gas flow (Nm <sup>3</sup> /hr)	1025	313473	332817	294118	18635	380000
	Mill fan flow (Nm <sup>3</sup> /hr)	1025	584992	685000	485000	74536	485000
	Grinding pressure (bar)	1025	70	90	50	14.7	50
	Separator speed (rpm)	1025	87	100	75	9.3	75
	Energy efficiency (%)	1025	68.78	77.78	61.34	4.2	77.78

## 2.3. ANFIS model building

A model was developed using five independent variables of plant operational data analysis: raw mill output (kg/hr), material moisture (kg/hr), kiln hot gas flow (Nm<sup>3</sup>/hr), mill fan flow (Nm<sup>3</sup>/hr), grinding pressure (bar) and separator speed (rpm). The output set contains data on energy efficiency. The data used to develop the comprehensive model so far is derived from plant operational data, primarily from the cement plant. Probability analysis is used during the data selection process. Potential outliers are eliminated following an analysis. A total of 1025 vertical raw mill plant operational data were used in this study based on this method. Three subsets of this data set are available: 717 for training, 154 for validation, and 154 for testing. These variables are listed in Table 2 along with their statistical characteristics. All subgroups have quite large ranges of data for each variable.

To construct model programs, Matlab functions linked to ANFIS are used (Demuth & Beale, 2000). In general, the fuzzy rules are described by a subject expert. However, when ANFIS is employed, the algorithm constructs the rules automatically rather than consulting an expert. In this study, three strategies for generating fuzzy inference system (FIS) structure from ANFIS data were studied. Grid partitioning (GP), subtractive clustering (SC), and fuzzy c-means (FCM) clustering are the approaches used. These strategies are used in this work to create and choose the optimum vertical raw mill energy efficiency prediction model.

For this study, a first-order Sugeno-type model was built using four input variables and IF-THEN fuzzy logic. Fuzzy rules, assuming two inputs (x, y) and one output (f), are as follows according to equations (12) and (13) of the fuzzy inference method (FIS):

$$Rule1 \rightarrow \text{if } x \text{ is } A_1 \text{ and } y \text{ is } B_1, \text{ then } f_1 = p_1x + q_1y + r_1 \quad (13)$$

$$\text{Rule2} \rightarrow \text{if } x \text{ is } A_2 \text{ and } y \text{ is } B_2, \text{ then } f_2 = p_2x + q_2y + r_2 \quad (14)$$

1) Layer 1: In this layer, we use the Membership function to convert fuzzification values into membership values, as shown in Eq. (15):

$$O_i^1 = \mu_{A_i}(x) \quad (15)$$

where  $x$  is the input to node  $i$  and  $A_i$  is the linguistic label associated with this node..

2) Layer 2: Every node in this layer reproduces the input and sends out the results. Thus, each node in the same layer can decide the firepower of a rule. Eq. (16) shows an example of this layer (Jang & Sun, 1995; Sadrmomtazi, Sobhani, & Mirgozar, 2013).

$$w_i = \mu_{A_i}(y) x \mu_{B_i}(y), i = 1, 2. \quad (16)$$

3) Layer 3: Membership values can be normalized using this layer. Throughout this layer, the  $i$ th node indicates how much firepower the  $i$ th law generates compared to the sum of all fire powers. A normalized firing force measurement for node  $i$ th is given by Eq. (17) below.

$$\bar{w}_i = \frac{w_i}{(w_1 + w_2)}, i = 1, 2. \quad (17)$$

4) Layer 4: This layer, also known as the adaptive layer, can define the relationship between the input and output values, as shown in Eq. (18)

$$O_i^4 = \bar{w}_i (p_i x + q_i y + r_i) \quad (18)$$

where  $\bar{w}_i$  is the output resulted from layer 3, and  $\{p_i + q_i + r_i\}$  is the parameter set.

5) Layer 5: Defuzzification is another name for this layer. As shown in Eq. (19), the later signal node calculates the total output as the sum of all input signals.

$$O_i^5 = \sum_i \bar{w}_i f_i = \frac{\sum_i w_i f_i}{\sum_i w_i} \quad (19)$$

## 2.3.1 PSO-ANFIS and GA-ANFIS weight optimization

In genetic algorithms, natural selection and genetic science combines together to create an evolutionary heuristic search algorithms. Thus, to solve optimization problems, it uses a random search method. As a result, GAs direct calls to the regions that actually perform better in the search area based on the information they have at their disposal. GA is primarily concerned with simulating natural systems, which have an evolutionary process. Throughout nature, the strongest individuals always dominate the weakest in competition for insufficient resources. There is a group of individuals within the search field for a GA representing a solution to a particular problem. The variables are the genes and these individuals are like chromosomes. An individual's "competition" ability, however, is determined by their eligibility score for each solution (Ganjidoost, Mousavi, & Soroush, 2016; Hasanipناه, Amnieh, Arab, & Zamzam, 2018; Rezakazemi, Dashti, Asghari, & Shirazian, 2017). Consequently, Particle swarm optimization (PSO) is a stochastic optimization method based on population. A fish or insect

moving in a swarm inspired the development of this algorithm (Kennedy & Eberhart, 1995). Iteratively updating generations seeks optimal solutions by selecting a population of random solutions. The best available solutions pass through the problem area as potential solutions, called particles in the PSO. Genetic algorithms (GAs) and PSOs have many similarities. Unlike the GA, the PSO does not incorporate evolutionary operators such as crossovers and mutations. In addition to its ease of implementation, the PSO has a low number of parameters to configure. Artificial intelligence tools have been optimized with PSO for various applications.

## 2.3.2. Grid partition method

The grid partition (GP) method constructs a Sugeno-type FIS structure with sigmoidal membership function  $\text{dsigmf}$  as its input membership function as shown in Fig. 4 above. It features five, four, three, and two membership function numbers for six input parameters (raw mill output, material moisture, kiln hot gas flow, mill fan flow, grinding pressure and separator speed). Furthermore, the output function is constant and the best rule number is 12. Prediction error increases dramatically when the output membership function is assumed to be linear. An excessive number of linear parameters causes this condition. Likewise, as the membership function number for each input parameter increases, so does the rule number. The simulation model is slowed as a result of this condition. According to a predetermined number of membership functions, GP divides the input data into a number of local fuzzy regions. Eight types of membership functions are used in the GP technique ( $\text{trimf}$ ,  $\text{trapmf}$ ,  $\text{gbellmf}$ ,  $\text{gaussmf}$ ,  $\text{gauss2mf}$ ,  $\text{pimf}$ ,  $\text{dsigmf}$ ,  $\text{psigmf}$ ). With a Sugeno in use, only one output is available, which can either be constant or linear, depending on the number of membership functions specified for each input. This approach generates same amount of rules as it does output membership functions. A variety of membership function features (types, numbers) are used in this subsection to construct alternate models consisting of distinct FIS structures, based on training data. In order to determine the most suitable alternative model, a number of simulation experiments are conducted. Different alternative model (for example, GA-ANFIS-GP1 and PSO-ANFIS-GP1) generates various sub-models. In this article, however, only the sub-model with the lowest RMSE, MAE, AAE, and other characteristics is presented as the best sub-model. This procedure is done for the remaining potential models (PSO-ANFIS-GP2, PSO-ANFIS-GP3, GA-ANFIS-GP2, GA-ANFIS-GP3, etc). Based on extensive simulations, Tables 4 and 5 shows all possible models' features and performance (RMSE, MAE, and AAE). According to the table, the best sub clustering-based energy efficiency prediction model is PSO-ANFIS-GP10 ( $R^2 = 0.9492$ , RMSE = 0.95795, MAE = 0.70843, AAE = 0.01048) and GA-ANFIS-GP3 ( $R^2 = 0.903$ , RMSE = 1.3306, MAE = 0.9255, AAE = 0.01375) which has the smallest error. Furthermore, with  $\text{trapMF}$  or  $\text{trimMF}$  type of output, influence the model outcomes, which diminishes significantly. As a result, the features  $\text{gaussMF}$  and linear/constant performance outcomes are not considerably different following the PSO-ANFIS-GP10 and GA-ANFIS-GP3 models.

Table 4  
Models with alternative PSO-ANFIS-GP features and performance results.

Model	Number of input MF	Type of input MF	Type of output MF	Epochs	R <sup>2</sup>	Error analysis		
						RMSE	MAE	AAE
PSO-ANFIS-GP1	[2 2 2]	gaussMF	constant	200	0.9304	1.1307	0.8829	0.01297
PSO-ANFIS-GP2	[2 2 2]	dsigMF	constant	200	0.9028	1.3261	1.0746	0.01575
PSO-ANFIS-GP3	[2 2 2]	trimMF	constant	200	0.8734	1.51545	1.168	0.01727
PSO-ANFIS-GP4	[2 2 2]	trapMF	constant	200	0.8593	1.60298	1.30526	0.01919
PSO-ANFIS-GP5	[2 2 2]	gaussMF	constant	250	0.906	1.31372	1.04636	0.01538
PSO-ANFIS-GP6	[2 2 2]	gaussMF	linear	200	0.884	1.44757	1.12604	0.01663
PSO-ANFIS-GP7	[2 2 2]	gaussMF	linear	180	0.939	1.0485	0.80966	0.01176
PSO-ANFIS-GP8	[2 2 2]	gaussMF	constant	150	0.924	1.17908	0.99611	0.01457
PSO-ANFIS-GP9	[2 2 2]	gaussMF	linear	200	0.9451	1.00048	0.73379	0.01082
<i>PSO-ANFIS-GP10</i>	<b>[3 2 3]</b>	<b>gaussMF</b>	<b>linear</b>	<b>220</b>	<b>0.9492</b>	<b>0.95795</b>	<b>0.70843</b>	<b>0.01048</b>

Table 5  
Models with alternative GA-ANFIS-GP features and performance results.

Model	Number of input MF	Type of input MF	Type of output MF	Epochs	R <sup>2</sup>	Error analysis		
						RMSE	MAE	AAE
GA-ANFIS-GP1	[2 2 2]	gaussMF	constant	220	0.8813	1.46559	1.10701	0.01625
GA-ANFIS-GP2	[2 2 2]	gaussMF	constant	250	0.8719	1.53574	1.11051	0.01625
<i>GA-ANFIS-GP3</i>	<b>[3 2 5]</b>	<b>gaussMF</b>	<b>constant</b>	<b>300</b>	<b>0.903</b>	<b>1.33061</b>	<b>0.92545</b>	<b>0.01375</b>
GA-ANFIS-GP4	[2 2 2]	dsigmf	constant	300	0.8717	1.5352	1.06611	0.01560
GA-ANFIS-GP5	[2 1 1]	gaussMF	constant	300	0.9025	1.33445	0.92651	0.01376
GA-ANFIS-GP6	[1 1 1]	gaussMF	constant	200	0.8694	1.57362	1.33975	0.01966
GA-ANFIS-GP7	[2 2 3]	dsigmf	constant	300	0.8982	1.49863	1.12194	0.01658
GA-ANFIS-GP8	[3 2 3]	dsigmf	constant	350	0.8948	1.53968	1.26571	0.01845

### 2.3.3. Sub-clustering method

According to the sub-clustering approach (SC), every data point can be considered a cluster center as shown in Fig. 3 above. Data points are clustered based on their proximity to each other, which is used to determine the probability degree that a particular data point will define the cluster center. An algorithm determines which data point has the best chance of being the first cluster center. Using radii from the first cluster center, it determines the location of the next data cluster and its center. The iteration process is repeated until all data is contained within the cluster center radii (Akkaya, 2016). The subtractive clustering algorithm has four parameters. Influence, squash factor, acceptable ratio, and rejected ratio are examples.

Manually adjusting the clustering settings yields the best GA-ANFIS and PSO-ANFIS structures based on the SC technique. The range of influence (RI) is modified from 0.12 to 0.15 with a 0.01 increment value, while the squash factor (SF) is adjusted from 1.3 to 1.5 with a 0.1 increment value. It does not have any positive effect to change the default accept and reject ratios, so they remain at 0.5 and 0.15. As a result, 8 different models are developed. The program assigns gauss and linear membership function types to input and output membership functions for the considered models. Sub-clustering parameters determine the membership function number and

any input variable's membership function number determines the number of rules. According to the Table 5 and 6 below, the best sub clustering-based energy efficiency prediction model is PSO-ANFIS-SC3 ( $R^2 = 0.9387$ , RMSE = 1.0522, MAE = 0.8654, AAE = 0.01272) and GA-ANFIS-SC2 ( $R^2 = 0.8737$ , RMSE = 1.52288, MAE = 1.09126, AAE = 0.01595) which has the smallest error. When RI and SF are set to 0.14 and 1.4, respectively, the model yields three rules. Furthermore, lower RI and SF values are associated with greater rule numbers. Furthermore, with lower RI levels, the influence of SF on model outcomes diminishes significantly. As a result, the features and performance outcomes are not considerably different following the PSO-ANFIS-SC3 and GA-ANFIS-SC2 models.

Table 6  
Models with alternative PSO-ANFIS-SC features and performance results..

Model	R1	SF	Number of input MF	Epochs	R <sup>2</sup>	Error analysis		
						RMSE	MAE	AAE
PSO-ANFIS-SC1	0.15	1.5	[2 2 2]	200	0.8968	1.36472	1.07685	0.01581
PSO-ANFIS-SC2	0.12	1.5	[2 2 2]	200	0.9058	1.30485	1.05645	0.01547
<i>PSO-ANFIS-SC3</i>	<b>0.13</b>	<b>1.5</b>	<b>[2 2 2]</b>	<b>200</b>	<b>0.9387</b>	<b>1.0522</b>	<b>0.86541</b>	<b>0.01272</b>
PSO-ANFIS-SC4	0.14	1.5	[2 2 2]	200	0.8921	1.39852	1.06451	0.0158
PSO-ANFIS-SC5	0.2	1.5	[2 2 2]	150	0.881	1.46483	1.13523	0.01676
PSO-ANFIS-SC6	0.25	1.5	[2 2 2]	180	0.9337	1.09561	0.86026	0.01263
PSO-ANFIS-SC7	0.25	1.5	[2 2 2]	200	0.9166	1.22865	1.00633	0.01474
PSO-ANFIS-SC8	0.18	1.5	[2 2 2]	180	0.9302	1.12319	0.90035	0.01321

Table 7  
Models with alternative GA-ANFIS-SC features and performance results..

Model	R1	SF	Number of input MF	Epochs	R <sup>2</sup>	Error analysis		
						RMSE	MAE	AAE
GA-ANFIS-SC1	0.15	1.5	[2 2 2]	200	0.8678	1.58918	1.3242	0.01945
<i>GA-ANFIS-SC2</i>	<b>0.3</b>	<b>1.5</b>	<b>[2 2 2]</b>	<b>200</b>	<b>0.8748</b>	<b>1.52288</b>	<b>1.09126</b>	<b>0.01595</b>
GA-ANFIS-SC3	0.12	1.5	[2 2 2]	200	0.8806	1.468	1.16489	0.01715
GA-ANFIS-SC4	0.25	1.5	[2 2 2]	300	0.8887	1.53387	1.30137	0.01894
GA-ANFIS-SC5	0.2	1.5	[2 2 2]	150	0.8681	1.57029	1.32245	0.01942
GA-ANFIS-SC6	0.25	1.5	[2 2 2]	180	0.8479	1.65868	1.26434	0.01871
GA-ANFIS-SC7	0.25	1.5	[2 2 2]	150	0.8828	1.45645	1.2067	0.01773

### 2.3.4. Fuzzy c-means method

A FIS structure is created using the Fuzzy C-means (FCM) clustering algorithm. This structure can generate rules based on data behavior. For the input and output variables, the FCM method is used to identify the number of rules and membership functions. FCM can be configured to generate any number of clusters you desire and this is usually more clusters if you choose a smaller cluster radius. This means that there will be more rules in the created FIS. When Sugeno is chosen as the FIS structure type, the input and output membership function types are gauss and linear, respectively. By varying the number of clusters, six different models are constructed (NC). The number of clusters dictates the number of MFs and rules. Simulations on these different models are run in order to determine the best FIS structure. Table 6 shows the model's attributes and performance results.

As seen in the Tables 8 and 9, additional clusters do not necessarily result in higher performance. The PSO-ANFIS-FCM8 model 8 clusters ( $R^2 = 0.9304$ , RMSE = 1.1296, MAE = 0.8305, AAE = 0.0123) and GA-ANFIS-FCM3 model 3 clusters ( $R^2 = 0.9028$ , RMSE = 1.3261, MAE = 1.0746, AAE = 0.01575) had the lowest error. As a result, the PSO-ANFIS-FCM8 model with four rules is regarded as the best. The model over-learns (fits) as the number of clusters increases.

Table 8  
Models with alternative PSO-ANFIS-FCM features and performance results..

Models	Number of clusters	Number of input MF	Number of output MF	Number of rule	Epochs	R <sup>2</sup>	Error analysis		
							RMSE	MAE	AAE
PSO-ANFIS-FCM1	2	[2 2 2]	[2]	2	200	0.8725	1.5192	1.2069	0.0178
PSO-ANFIS-FCM2	3	[3 3 3]	[3]	3	200	0.8919	1.3995	1.0986	0.0161
PSO-ANFIS-FCM3	4	[4 4 4]	[4]	4	180	0.8959	1.3699	1.1212	0.0165
PSO-ANFIS-FCM4	5	[5 5 5]	[5]	5	180	0.9036	1.3222	1.0125	0.0150
PSO-ANFIS-FCM5	6	[6 6 6]	[6]	6	150	0.9244	1.1672	0.8882	0.0131
PSO-ANFIS-FCM6	7	[7 7 7]	[7]	7	120	0.9067	1.3012	0.9969	0.0146
<i>PSO-ANFIS-FCM7</i>	<b>8</b>	<b>[8 8 8]</b>	<b>[8]</b>	<b>8</b>	<b>140</b>	<b>0.9304</b>	<b>1.1296</b>	<b>0.8305</b>	<b>0.0123</b>
PSO-ANFIS-FCM8	9	[9 9 9]	[9]	9	130	0.8971	1.3684	1.0440	0.0155



Table 9  
Models with alternative GA-ANFIS-FCM features and performance results.

Models	Number of clusters	Number of input MF	Number of output MF	Number of rule	Epochs	R <sup>2</sup>	Error analysis		
							RMSE	MAE	AAE
GA-ANFIS-FCM1	2	[2 2 2]	[2]	2	200	0.8745	1.5168	1.1194	0.01635
<i>GA-ANFIS-FCM2</i>	<b>3</b>	<b>[3 3 3]</b>	<b>[3]</b>	<b>3</b>	<b>200</b>	<b>0.8964</b>	<b>1.4261</b>	<b>1.0746</b>	<b>0.01575</b>
GA-ANFIS-FCM3	4	[4 4 4]	[4]	4	150	0.8847	1.4798	1.1252	0.01663
GA-ANFIS-FCM4	5	[5 5 5]	[5]	5	100	0.8674	1.5862	1.3295	0.01949
GA-ANFIS-FCM5	6	[6 6 6]	[6]	6	180	0.8863	1.5376	1.2827	0.01871
GA-ANFIS-FCM6	7	[7 7 7]	[7]	7	180	0.8871	1.5441	1.2848	0.01875

### 3.0 Results and discussion

Based upon reference plant data, the process simulator was used to identify areas for improving the cement vertical raw mill plant's energy efficiency. Table 10 shows both the inlet and outlet streams of the vertical raw mill process and their mass and energy balances. According to Table 3, the cement vertical raw mill system has an energy efficiency of 67.3 percent. Energy efficiency percentages in this study followed a similar pattern, with estimated values between 60 and 70%. According to the Aspen Plus process simulator (Table 3), the material moisture drying unit loses a significant amount of energy. This was primarily due to the drying process that occurs in the grinding unit, with inlet material moisture ranging from 20 to 25% and ground material moisture of less than 1%. This is done to prevent moist product from clogging the transport system and silo cake-up during ex-mill product storage. As a result of this, moisture mass flow has a significant impact on energy efficiency (Atmaca & Kanoglu, 2012). Drying unit is one of the major thermodynamic inefficiencies in vertical raw mills (Ghalandari et al., 2021).

Table 10  
Simulated data for energy analysis of a cement vertical raw mill.

Equipment/ N° of input stream	Mass (kg/kg raw mix)	Energy (kJ/kg)	Equipment/ N° of output stream	Mass (kg/kg raw mix)	Energy (kJ/kg)
Raw material (1)	1.05	1251.14	Ex-mill Product exit (36)	1.00	363.57
Combustion air (2)	0.44	82.55	GCT exit (31)	0.06	1577.33
Hot gas generator (4)	0.01	4816.55	ESP exhaust (33)	2.58	4881.65
Material moisture (10)	0.33	1584.35			
Kiln hot gas flow (37)	1.81	2440.29			
Total	3.64	10174.88	Total	3.64	6822.55
Energy Efficiency	67.05%				

N°-Number; Process flow sheet Fig. 2 shows 1, 2, 4, 10, 31, 33, 36, and 37.

### 3. 1. Model testing results and discussion

A modeling approach using artificial intelligence assists scientists in understanding how a set of variables or properties influence a determinant variable in multiple, nonlinear ways. Based on three methods of generating FIS from the vertical raw mill operations data set in the model building section, PSO-ANFIS-GP4, PSO-ANFIS-SC5, and PSO-ANFIS-FCM3 are the optimal models. Additionally, the model performance of the PSO-ANFIS-FCM, PSO-ANFIS-GP, PSO-ANFIS-SC, GA- ANFIS-FCM, GA- ANFIS-GP and GA-ANFIS-SC approaches for the training and validation databases was also discussed and compared based on plant operation parameter data of a vertical raw mill. Afterwards, each input is analyzed to determine its relative importance. Through the use of reliable optimization algorithms, the predictive capacity of the model can be significantly improved. This study utilized PSO and GA algorithms in order to train ANFIS-FCM, ANFIS-GP and ANFIS-SC. The PSO values were fitted in the PSO- ANFIS-FCM, PSO- ANFIS-GP and PSO-ANFIS-SC through a comprehensive parametric study. As a hybrid algorithm, the PSO algorithm's output data is highly dependent on its input data. Consequently, the PSO algorithm is remarkably effective at handling nonlinear problems. The membership function (MF) utilized in this work was Gaussian. The best parameters were also determined by trial-and-error. Table 2 shows the optimal parameters for the PSO algorithm. Similar to the PSO-ANFIS model, GA-ANFIS-FCM, GA-ANFIS-GP, and GA-ANFIS-SC models used the Gaussian membership function. The MATLAB package was used to simulate the model. Similarly to PSO, we optimized various important GA parameters in order to obtain the best results. Tracking model performance with different GA parameters was again performed using the trial-and-error method.

Here we are determining the best GA-ANFIS and PSO-ANFIS model from the optimal ones obtained. In the testing phase, these generated models are evaluated for their prediction abilities so that the best optimal ANFIS model can be found. A performance criterion provides an evaluation of how closely the model prediction corresponds to the actual outcome. The remaining 154 data will be used in the testing phase. For each ANFIS model, Fig. 2 illustrates actual energy efficiency versus prediction results. Compared to actual results, the prediction results are

quite consistent. Among the six models, PSO-ANFIS-SC5 has the highest correlation coefficient, with better differentiation between them as shown in Fig. 3.

## 3.2. Model performance evaluation

A variety of statistical quality measurement methods were used to determine the precision of the model results.

The PSO- ANFIS-FCM, PSO- ANFIS-GP, PSO-ANFIS-SC, GA-ANFIS-FCM, GA-ANFIS-GP, and GA-ANFIS-SC models were evaluated using the root mean square error (RMSE), mean absolute error (MAE), and average absolute error (AAE) between actual and predicted energy efficiency as shown in Eq. 20 to 23:

$$R^2 = 1 - \frac{\sum_{i=1}^n (E_{i,estd} - E_{i,meas})^2}{\sum_{i=1}^n (E_{i,meas} - E_{meas,mean})^2} \quad (20)$$

$$RMSE = \sqrt{\frac{\sum_{i=1}^n (E_{i,meas} - E_{i,estd})^2}{n}} \quad (21)$$

$$MAE = \frac{1}{n} \sum_{i=1}^n |E_{i,meas} - E_{i,estd}| \quad (22)$$

$$AAE = \frac{1}{n} \sum_{i=1}^n \left| \frac{E_{i,meas} - E_{i,estd}}{E_{i,meas}} \right| \quad (23)$$

The first method entails plotting estimated energy efficiency data against plant operational energy efficiency data. As shown in Figs. 5 and 6, the plotted data are sufficiently adjacent to the line, implying that the model predicted and the measured energy efficiency data agree. The  $R^2$  of prognostication of the best models was 0.9492, 0.9387, 0.9304, 0.903, 0.8964, and 0.8737, respectively, for the PSO-ANFIS-GP10, PSO-ANFIS-SC3, PSO-ANFIS-FCM7, GA- ANFIS-GP3, GA-ANFIS-FCM2 and GA-ANFIS-SC2 models, which is a criterion of precision for the models. The RMSE, MAE, AAE, and  $R^2$  were used to evaluate the predictions of the developed models. Models presented in Table 11 have statistical properties that support their reliability, including a high  $R^2$  value and low RMSE, MAE, and AAE magnitudes. As a result, the PSO-ANFIS-GP10, PSO-ANFIS-SC3, PSO-ANFIS-FCM7 models are superior. The outputs of the predicted model was compared to the outputs of the process simulator energy efficiency evaluated. Table 5 contains the formulas for these correlations. The comparison confirms the model developed in this study's high precision.

Based on the comparison, it was found that the PSO-ANFIS-GP10 model outperformed other models based on the lowest AAE value it could estimate for the entire dataset.

Table 11  
The features and performance results of the best of ANFIS models

Models	Epochs	R <sup>2</sup>	Error analysis		
			RMSE	MAE	AAE
PSO-ANFIS-GP10	220	0.9492	0.95795	0.70843	0.01048
PSO-ANFIS-SC3	200	0.9387	1.0522	0.86541	0.01272
PSO-ANFIS-FCM7	140	0.9304	1.1296	0.83049	0.01227
GA-ANFIS-GP3	300	0.903	1.33061	0.925448	0.013746
GA-ANFIS-SC2	200	0.8737	1.52288	1.09126	0.01595
GA-ANFIS-FCM2	190	0.9028	1.32611	1.07461	0.01575

### 3.3. The influence of key operational parameters on energy efficiency

Three major independent variables should be optimized to increase a VRM's first law efficiency and reduce its power consumption: separator speed, grinding pressure, and mill gas flow rate. Furthermore, VRM separator speed (rpm) is one of the key operational parameters that determines product particle size. Increasing the classifier rotor speed from 60 to 80 rpm decreases the particle size of the product from 16.5 to 10.6% residue on 90µm sieve (Altun et al., 2017). In contrast, increasing the separator speed from 60 to 80 rpm at a constant grinding pressure results in a reduced raw material production rate from 240,000 kg/h to 230,000 kg/h and which invariably, reduce the VRM energy efficiency from 68.0 to 67.4% of raw material. Moreover, decreasing the separator speed housing classifier results in temporary increase in first law of thermodynamic efficiency as shown in Fig. 11. Consequently, if a finer product becomes the target, the VRM's energy efficiency values will be on downward trend. It is noteworthy to mention that vertical raw mill performance is largely affected by the amount of circulating load in the internal grinding classifying circuit. As a result of particle loading and gas flow within the VRM, this load is managed by adjusting the pressure drop across the VRM. This reflects in the drop of the mill differential pressure, as the separator speed housing the classifier increases, resulting in the particle bed's height increase. Further increase in the mill pressure drop, leading to creating more internal grinding circuits, which lowers the VRM product rate and reduces the system energy efficiency. When the grinding pressure is increased, the product particle size changes slightly due to a change in compressive force impact between the materials and the rollers on the grinding table. This is an important parameter that can affect grinding efficiency of a VRM as shown in Fig. 8. Additionally, the production rate increases with the energy efficiency by moderately increasing the grinding pressure, as shown in Fig. 12. From both the surface and contour plot, as shown in Fig. 12, increasing the grinding pressure from 60 to 80 bar raises the raw material production rate from 240,000 kg/h to 248,000 kg/h as well as the energy efficiency with a merging of 0.58%. By increasing grinding pressure, finer particles are produced, which leave the classifying circuit more quickly, increasing grinding efficiency. In order to achieve the increased product rate, the particle size of the product is decreased, and reject materials that may be difficult to be lifted by mill fan flow to the classifier are reduced, causing the rate to increase. Consequently, the mill's motor should be protected against damage by adjusting the grinding pressure. Furthermore, an important operational parameter which influence the VRM performance is also the quantity of gas entering the mill, which is determined by the gas temperature, pressure drop across the

mill, and raw material moisture content. Figure 9 shows that the product particle size varies from 620,000 to 560,000 Nm<sup>3</sup>/h (gas flow), ranging between 90µm = 16.3% and 90µm = 16.9%. Furthermore, Fig. 13 depict the relationship between gas flow changes and the raw mill output (kg/h) with effect on VRM unit's energy efficiency, respectively. The raw material production rate fluctuates between 200,000 kg/h and 230,000 kg/h, after dropping the gas flow from 620,000 to 560,000 Nm<sup>3</sup>/h (Fig. 14), but the energy efficiency of the VRM production process decreases by approximately 12.8 percent due to the reduced fan motor power consumption. In addition, lowering the flow rate below 560,000 Nm<sup>3</sup>/h increases the pressure drop, and therefore the efficiency of internal grinding circuits, reducing the energy efficiency of the process. The raw material production rate decreases by 20,000 kg/h as a result of this variation, while the energy efficiency decreases by 0.25%. Consequently, the VRM unit's energy efficiency should be increased by optimizing the gas flow.

## 4.0. Conclusion

This study uses the PSO-ANFIS-FCM, PSO-ANFIS-GP, PSO-ANFIS-SC, GA-ANFIS-FCM, GA-ANFIS-GP, GA-ANFIS-SC models to predict the energy efficiency of a vertical raw mill based on output (kg/h), material moisture (kg/h), kiln hot gas flow (Nm<sup>3</sup>/hr), mill fan flow (Nm<sup>3</sup>/hr), grinding pressure (bar), and separator speed (rpm). To develop the proposed models, 1025 plant operating data was collected over a range of 2020 to 2021 of a steady state operating data to avoid a misrepresentation of data. The findings indicate that the PSO-ANFIS-GP10, PSO-ANFIS-SC3, PSO-ANFIS-FCM7 algorithms have high potential for use in vertical roller mill energy efficiency prediction. Furthermore, the PSO-ANFIS-GP10 model has the highest precision when compared to other model in the study. It shows that the low moisture and high raw feed of VRM as inputs help to increase the process' energy efficiency. Cement grinding processes can benefit from the use of models for estimating the energy efficiency of VRMs. Future experimental data can also be used to improve the performance of the models presented and develop more advanced models to also predict the efficiency of the second law of thermodynamics (exergy efficiency). In addition, the VRM product residue can also be studied extensively as it relates to the vertical raw mill specific power consumption.

## Declarations

### Declaration of Competing Interest

The authors have no relevant financial or non-financial interests to disclose.

## References

1. Akkaya, E. (2016). ANFIS based prediction model for biomass heating value using proximate analysis components. *Fuel*, 180, 687-693.
2. Altun, D., Benzer, H., Aydogan, N., & Gerold, C. (2017). Operational parameters affecting the vertical roller mill performance. *Minerals Engineering*, 103, 67-71.
3. Asadi, M., Guo, H., & McPhedran, K. (2020). Biogas production estimation using data-driven approaches for cold region municipal wastewater anaerobic digestion. *Journal of environmental management*, 253, 109708.

4. Atmaca, A., & Kanoglu, M. (2012). Reducing energy consumption of a raw mill in cement industry. *Energy*, 42(1), 261-269.
5. Bao, Y., Zhu, Y., Du, W., Zhong, W., & Qian, F. (2019). A distributed PCA-TSS based soft sensor for raw meal fineness in VRM system. *Control Engineering Practice*, 90, 38-49.
6. Bejan, A. (2016). *Advanced engineering thermodynamics*: John Wiley & Sons.
7. Cai, W., Liu, C., Lai, K.-h., Li, L., Cunha, J., & Hu, L. (2019). Energy performance certification in mechanical manufacturing industry: A review and analysis. *Energy Conversion and Management*, 186, 415-432.
8. Demuth, H., & Beale, M. (2000). *Neural network toolbox for use with MATLAB*.
9. Fernandes, H., Halim, A., & Wahab, W. (2019). *Modeling Vertical Roller Mill Raw Meal Residue by Implementing Neural Network*. Paper presented at the 2019 IEEE International Conference on Innovative Research and Development (ICIRD).
10. Ganjidoost, H., Mousavi, S. J., & Soroush, A. (2016). Adaptive network-based fuzzy inference systems coupled with genetic algorithms for predicting soil permeability coefficient. *Neural Processing Letters*, 44(1), 53-79.
11. Ghalandari, V., Esmailpour, M., Payvar, N., & Reza, M. T. (2021). A case study on energy and exergy analyses for an industrial-scale vertical roller mill assisted grinding in cement plant. *Advanced Powder Technology*, 32(2), 480-491.
12. Ghalandari, V., & Iranmanesh, A. (2020). Energy and exergy analyses for a cement ball mill of a new generation cement plant and optimizing grinding process: A case study. *Advanced Powder Technology*, 31(5), 1796-1810.
13. Ghalandari, V., Majd, M. M., & Golestanian, A. (2019). Energy audit for pyro-processing unit of a new generation cement plant and feasibility study for recovering waste heat: A case study. *Energy*, 173, 833-843.
14. Gong, Y., Yuan, Z., Liu, Z., & Feng, Z. (2019). *Modeling for Cement Combined Grinding Process System Based on RBF Neural Network*. Paper presented at the 2019 IEEE 3rd Advanced Information Management, Communicates, Electronic and Automation Control Conference (IMCEC).
15. Hasanipanah, M., Amnieh, H. B., Arab, H., & Zamzam, M. S. (2018). Feasibility of PSO–ANFIS model to estimate rock fragmentation produced by mine blasting. *Neural Computing and Applications*, 30(4), 1015-1024.
16. Inapakurthi, R. K., Miriyala, S. S., & Mitra, K. (2020). Recurrent neural networks based modelling of industrial grinding operation. *Chemical engineering science*, 219, 115585.
17. Jang, J.-S., & Sun, C.-T. (1995). Neuro-fuzzy modeling and control. *Proceedings of the IEEE*, 83(3), 378-406.
18. Kennedy, J., & Eberhart, R. (1995). Particle swarm optimization. *IEEE Int Conf Neural Netw* 4: 1942–1948.
19. Kong, L., Price, L., Hasanbeigi, A., Liu, H., & Li, J. (2013). Potential for reducing paper mill energy use and carbon dioxide emissions through plant-wide energy audits: A case study in China. *Applied energy*, 102, 1334-1342.
20. Kumar, M., Singh, G., Arya, S. K., Bhatti, J. S., & Sharma, P. (2018). Artificial Neuro-Fuzzy Inference System (ANFIS) based validation of laccase production using RSM model. *Biocatalysis and Agricultural Biotechnology*, 14, 235-240.
21. Noori, R., Hoshyaripour, G., Ashrafi, K., & Araabi, B. N. (2010). Uncertainty analysis of developed ANN and ANFIS models in prediction of carbon monoxide daily concentration. *Atmospheric Environment*, 44(4), 476-

22. Okoji, A. I., Anozie, A. N., & Omoleye, J. A. (2021). Evaluation of optimization techniques for predicting exergy efficiency of the cement raw meal production process. *Cogent Engineering*, 8(1), 1930493.
23. Okoji, A. I., Anozie, A. N., & Omoleye, J. A. (2022a). Evaluating the thermodynamic efficiency of the cement grate clinker cooler process using artificial neural networks and ANFIS. *Ain Shams Engineering Journal*, 13(5), 101704.
24. Okoji, A. I., Anozie, A. N., Omoleye, J. A., Taiwo, A. E., & Osuolale, F. N. (2022b). Energetic assessment of a precalcining rotary kiln in a cement plant using process simulator and neural networks. *Alexandria Engineering Journal*, 61(7), 5097-5109.
25. Okoji, A. I., Babatunde, D. E., Anozie, A. N., & Omoleye, J. A. (2018). *Thermodynamic analysis of raw mill in cement industry using aspen plus simulator*. Paper presented at the IOP Conference Series: Materials Science and Engineering.
26. Okoji, C. N., Okoji, A. I., Ibrahim, M. S., & Obinna, O. (2022). Comparative analysis of adaptive neuro-fuzzy inference system (ANFIS) and RSRM models to predict DBP (trihalomethanes) levels in the water treatment plant. *Arabian Journal of Chemistry*, 15(6), 103794.
27. Pani, A. K., & Mohanta, H. K. (2014). Soft sensing of particle size in a grinding process: Application of support vector regression, fuzzy inference and adaptive neuro fuzzy inference techniques for online monitoring of cement fineness. *Powder technology*, 264, 484-497.
28. Pani, A. K., & Mohanta, H. K. (2015). Online monitoring and control of particle size in the grinding process using least square support vector regression and resilient back propagation neural network. *ISA transactions*, 56, 206-221.
29. Rezakazemi, M., Dashti, A., Asghari, M., & Shirazian, S. (2017). H<sub>2</sub>-selective mixed matrix membranes modeling using ANFIS, PSO-ANFIS, GA-ANFIS. *International Journal of Hydrogen Energy*, 42(22), 15211-15225.
30. Sadrmomtazi, A., Sobhani, J., & Mirgozar, M. (2013). Modeling compressive strength of EPS lightweight concrete using regression, neural network and ANFIS. *Construction and Building Materials*, 42, 205-216.
31. SCHÄFER, H.-U. (2002). Slag grinding: latest advances. *World cement*, 33(9), 61-66.
32. Shamshirband, S., Hadipoor, M., Baghban, A., Mosavi, A., Bukor, J., & Várkonyi-Kóczy, A. R. (2019). Developing an ANFIS-PSO model to predict mercury emissions in combustion flue gases. *Mathematics*, 7(10), 965.
33. Simmons, M., Gorby, L., & Terembula, J. (2005). *Operational experience from the United States' first vertical roller mill for cement grinding*. Paper presented at the Conference Record Cement Industry Technical Conference, 2005.
34. Tsakalakis, K. G., & Stamboltzis, G. A. (2008). Correlation of the Blaine value and the d<sub>80</sub> size of the cement particle size distribution. *ZKG international*, 61(3), 60.
35. Uzuner, S., & Çekmecelioğlu, D. (2016). Comparison of artificial neural networks (ANN) and adaptive neuro-fuzzy inference system (ANFIS) models in simulating polygalacturonase production. *BioResources*.
36. Wang, H., Jia, M.-p., Huang, P., & Chen, Z.-l. (2010). A study on a new algorithm to optimize ball mill system based on modeling and GA. *Energy Conversion and Management*, 51(4), 846-850.

37. Worrell, E., Martin, N., & Price, L. (2000). Potentials for energy efficiency improvement in the US cement industry. *Energy*, 25(12), 1189-1214.
38. Zhang, Q., Zhao, X., Lu, H., Ni, T., & Li, Y. (2017). Waste energy recovery and energy efficiency improvement in China's iron and steel industry. *Applied energy*, 191, 502-520.

## Figures

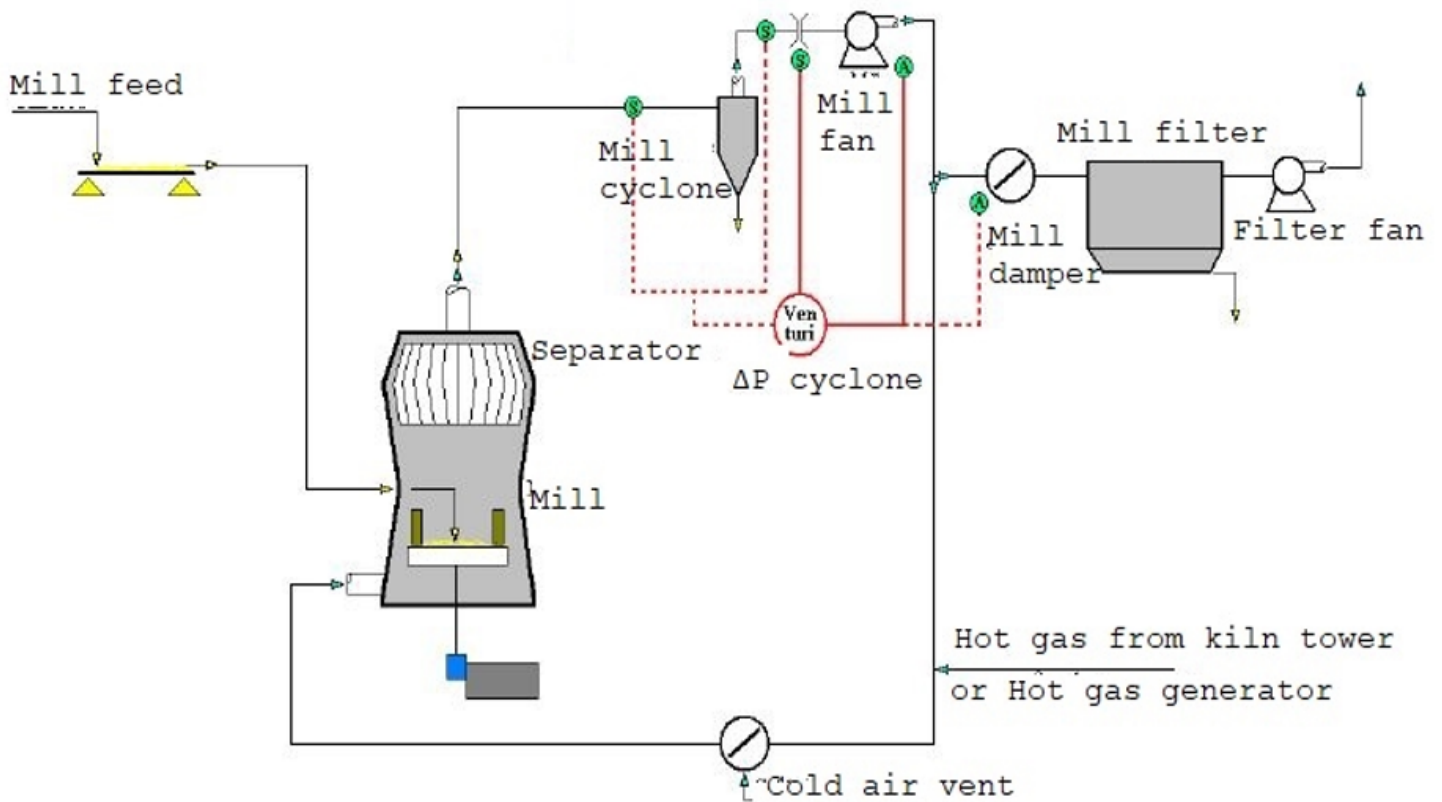
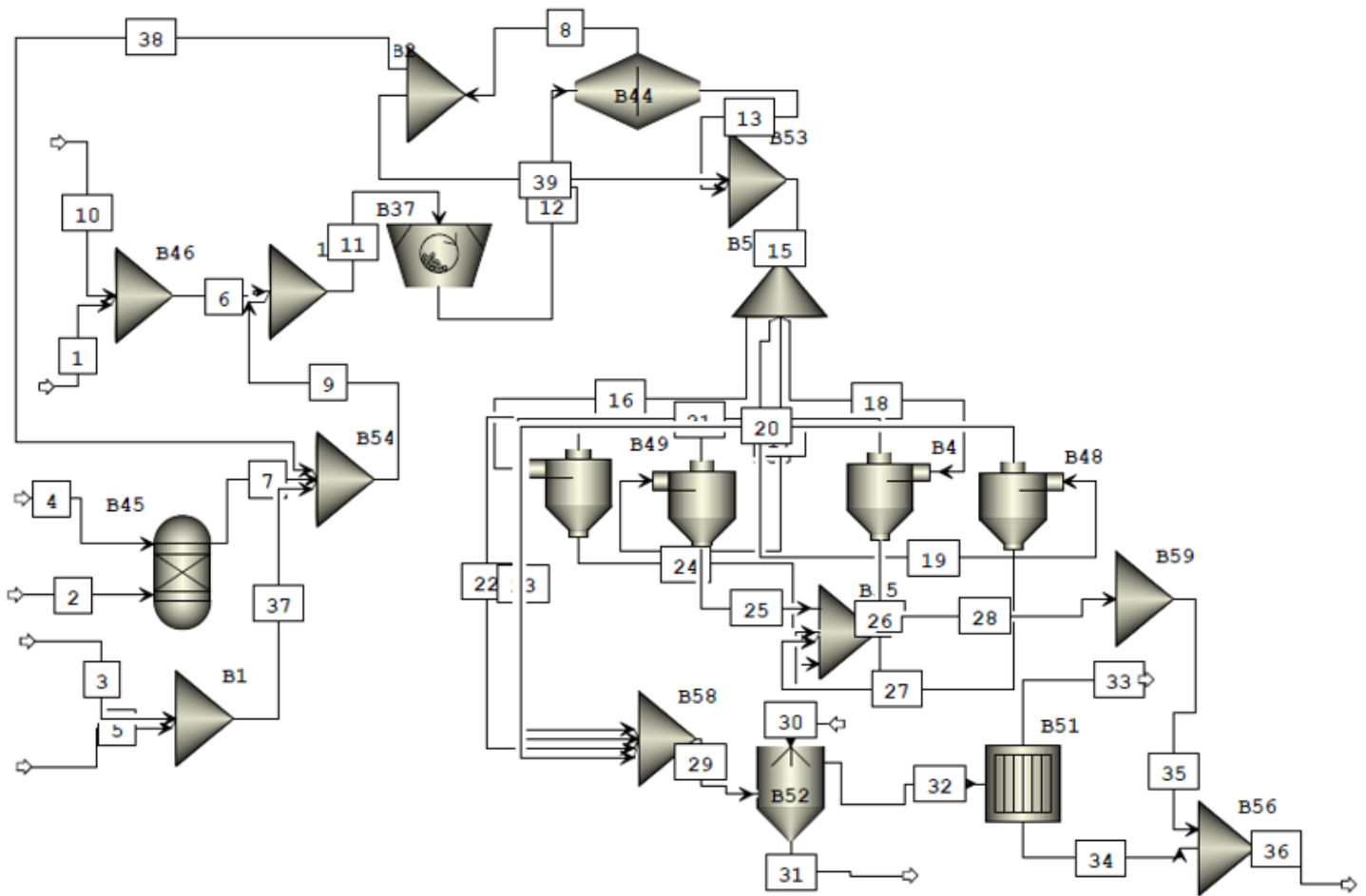


Figure 1

Vertical raw mill process flow diagram





**Figure 2**

Process flow sheet for cement vertical raw mill production represented with Aspen Plus process model (A. I. Okoji *et al.*, 2021)

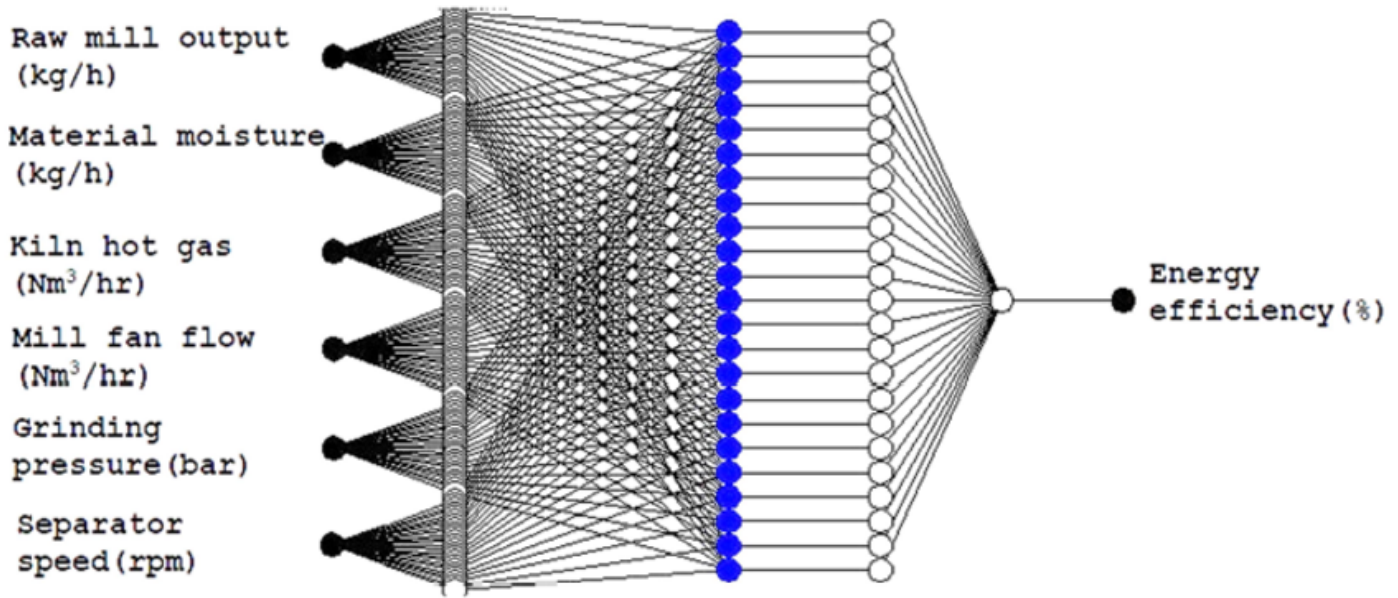


Figure 3

Architecture diagram of Subtractive clustering (SC)

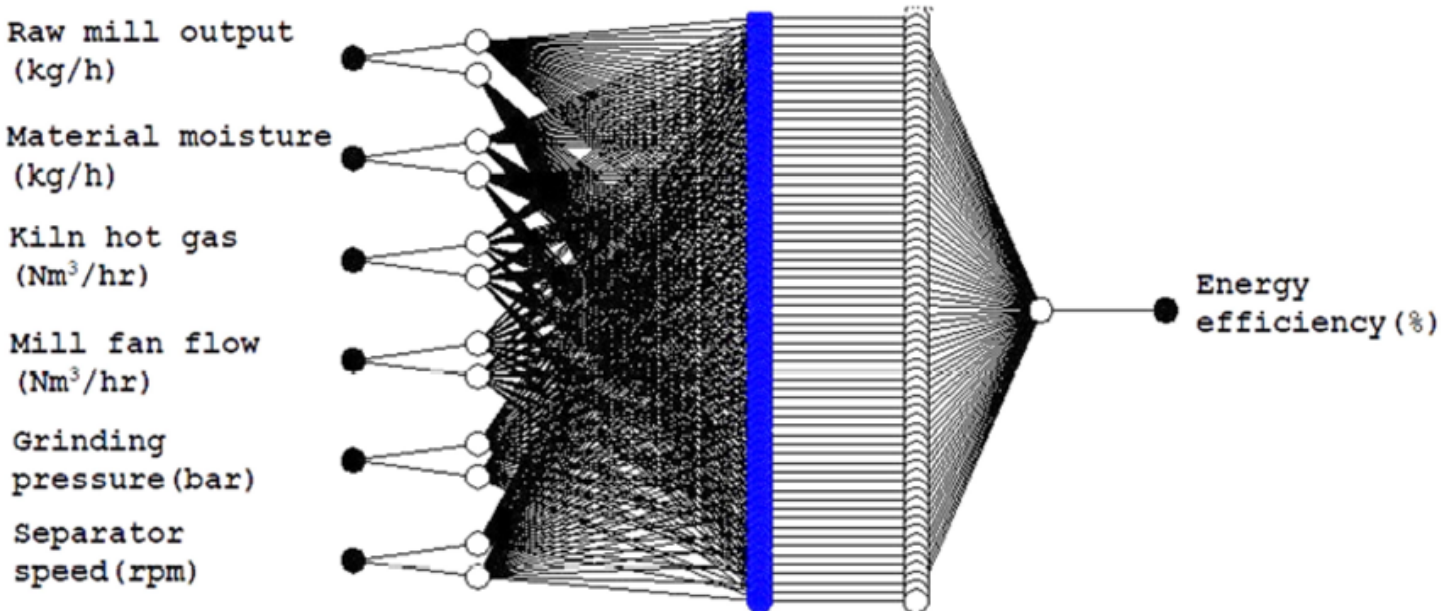


Figure 4

Architecture diagram representing Grid partitioning (GP)

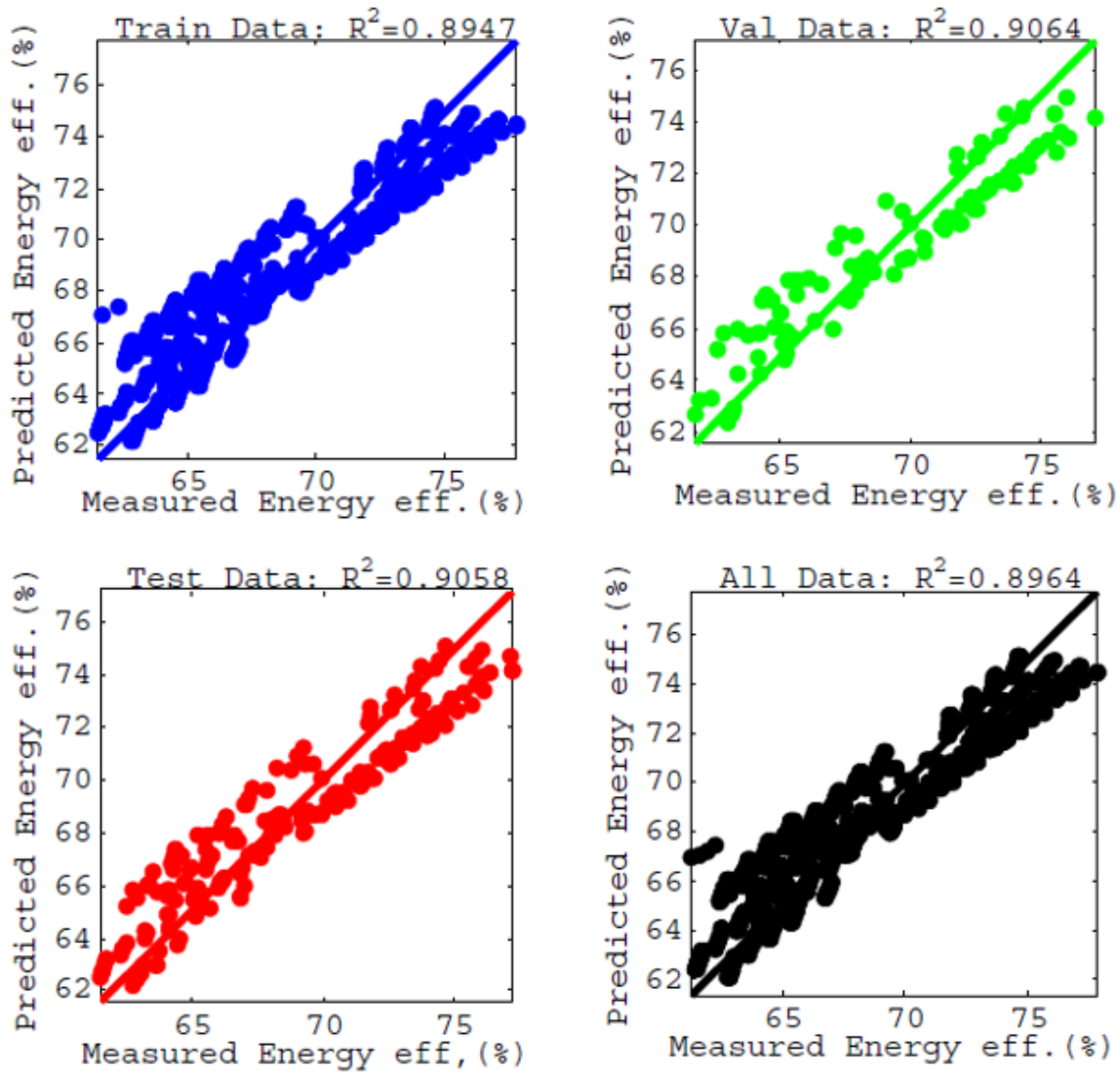


Figure 5

Comparison of predicted and measured energy efficiency values for GA-ANFIS-FCM2

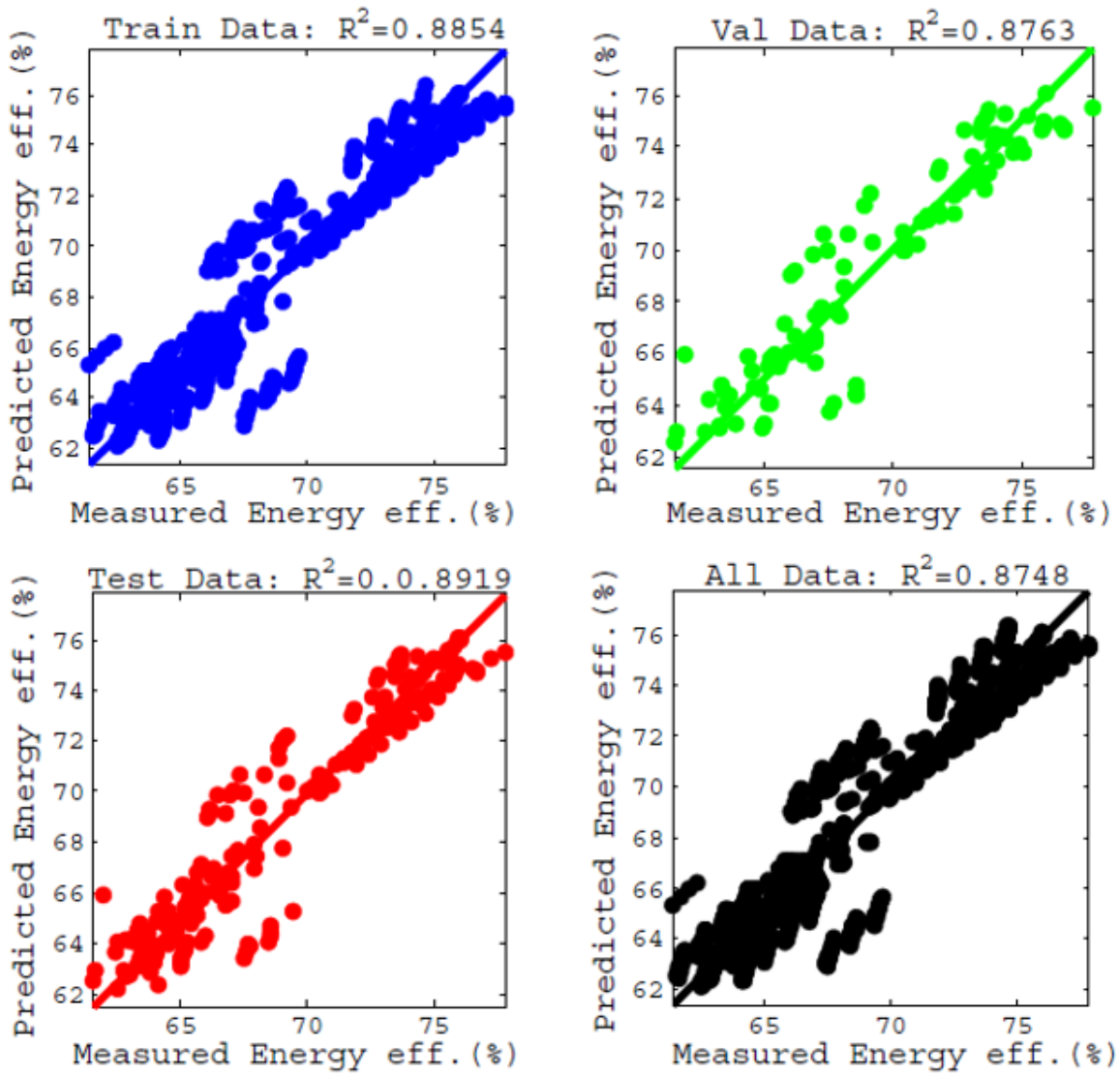


Figure 6

Comparison of predicted and measured energy efficiency values for GA-ANFIS-SC2

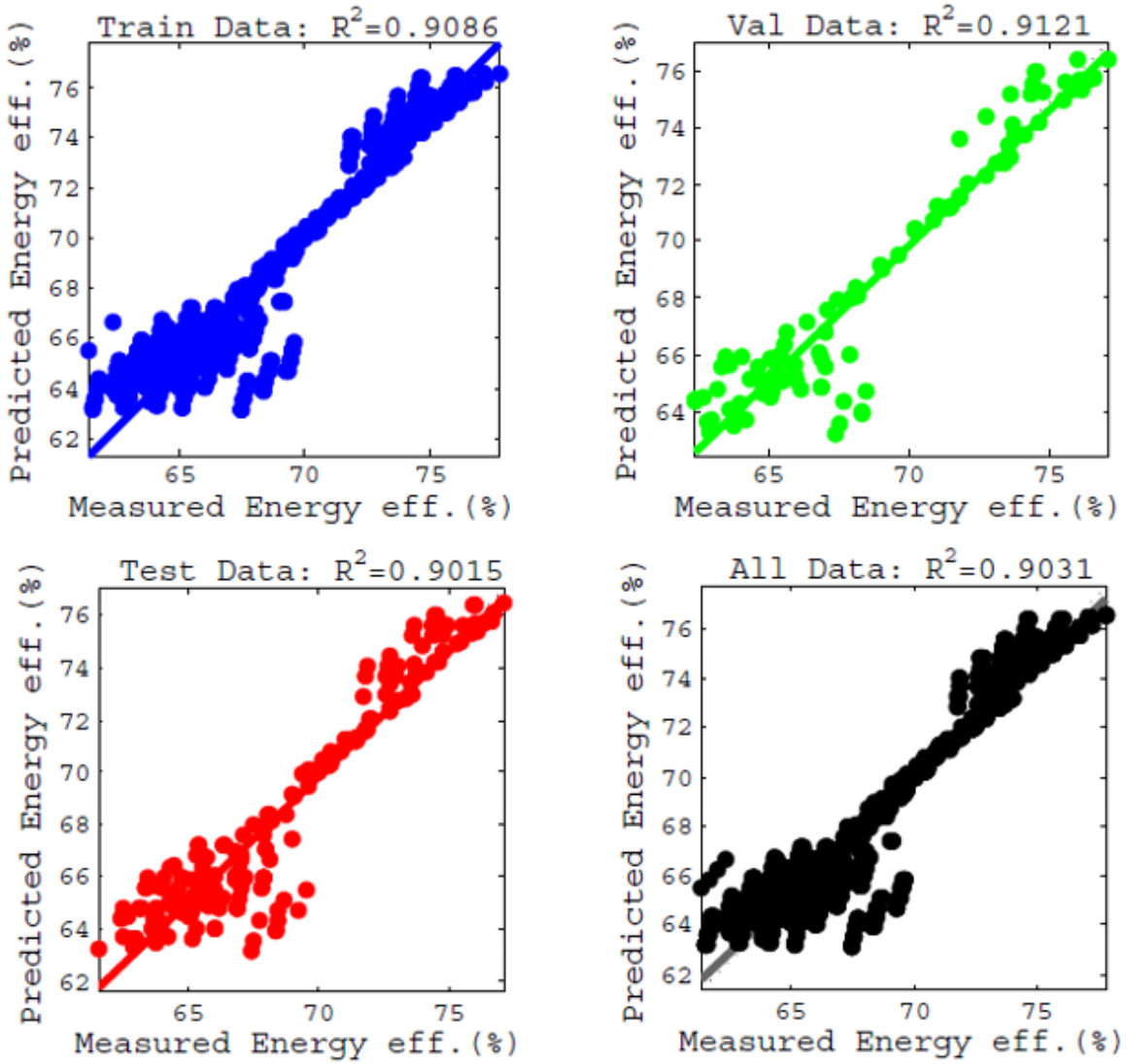
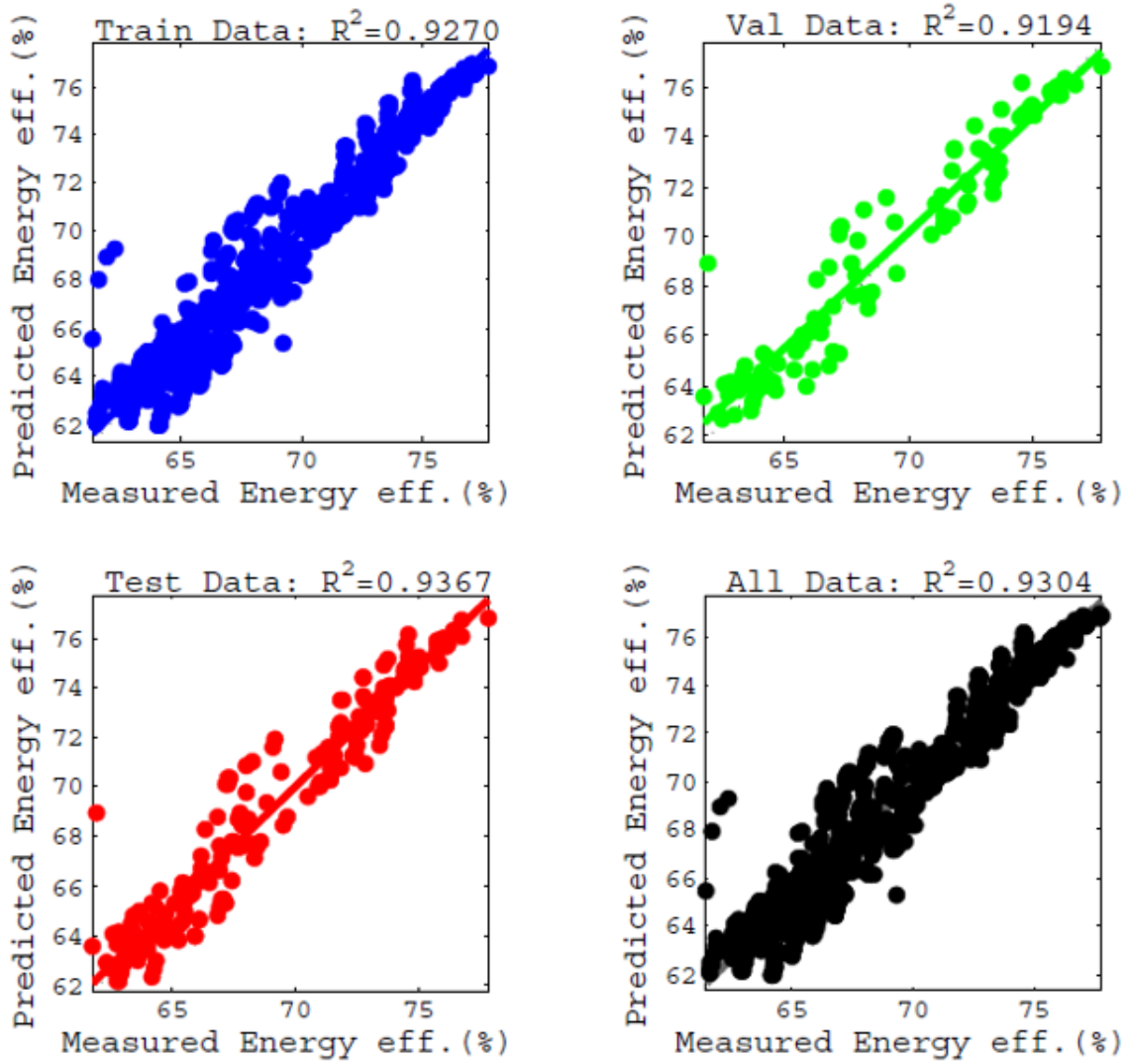


Figure 7

Comparison of predicted and measured energy efficiency values for GA-ANFIS-GP3



**Figure 8**

Comparison of predicted and measured energy efficiency values for PSO-ANFIS-FCM7

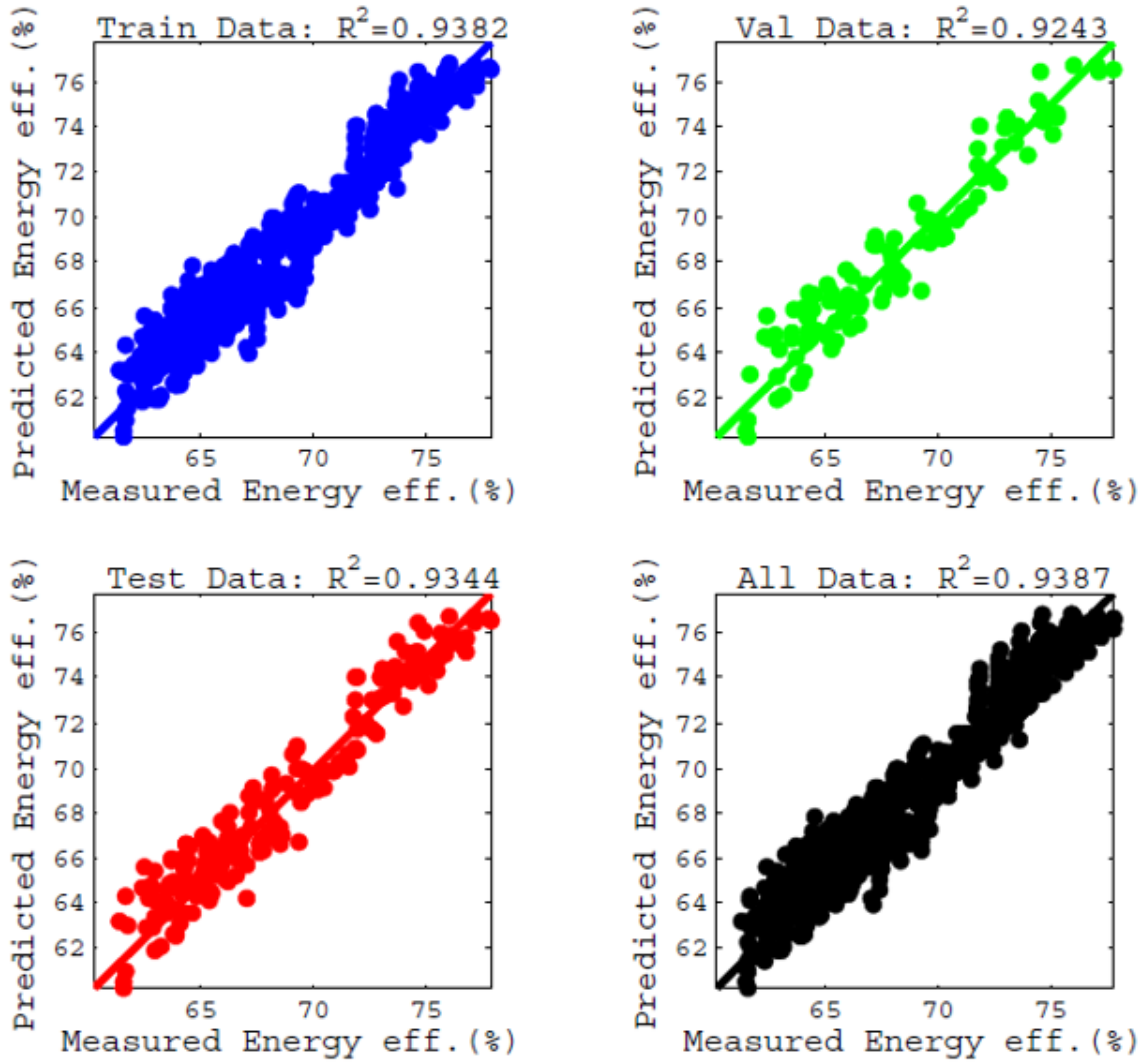


Figure 9

Comparison of predicted and measured energy efficiency values for PSO-ANFIS-SC3,



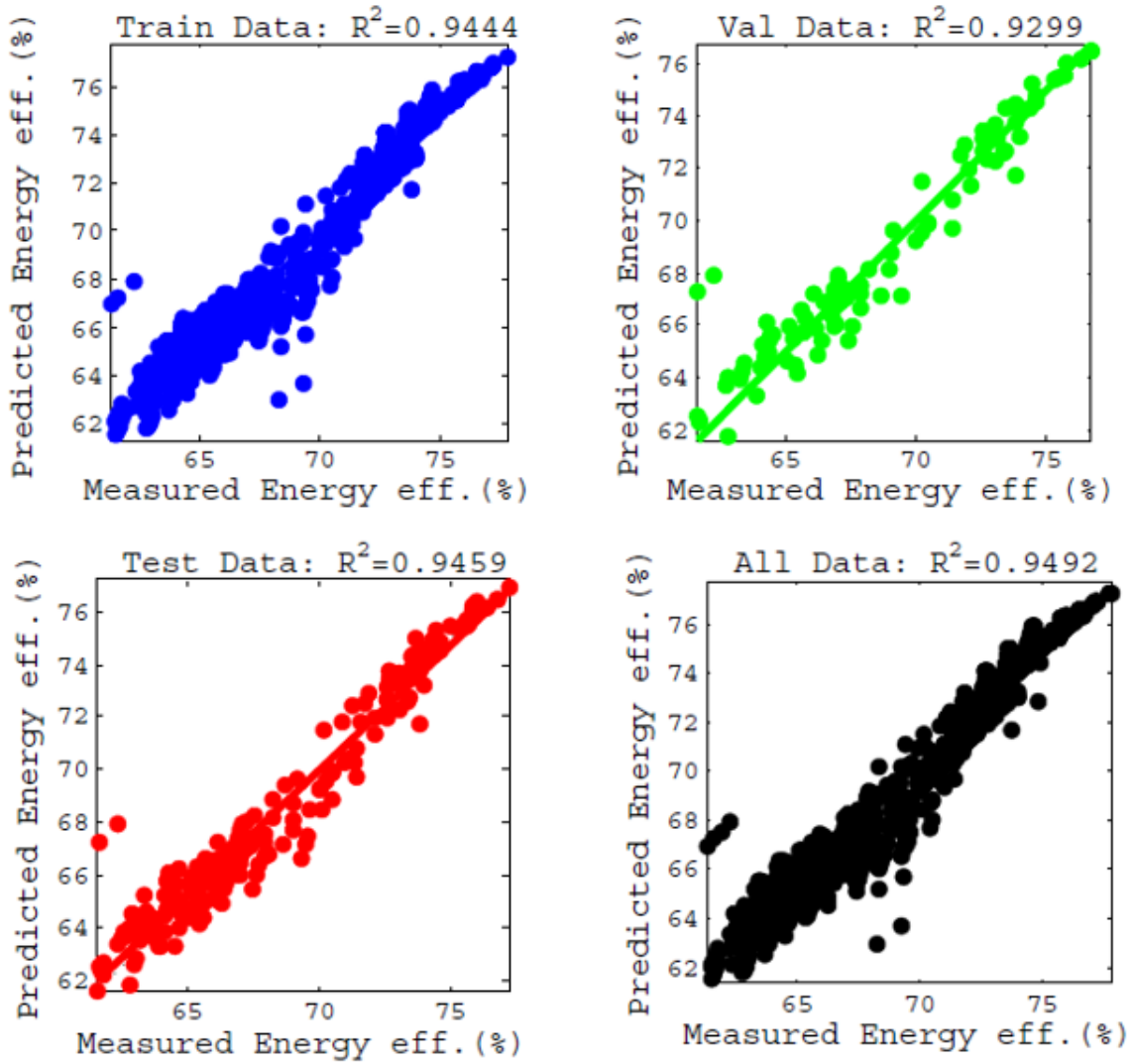
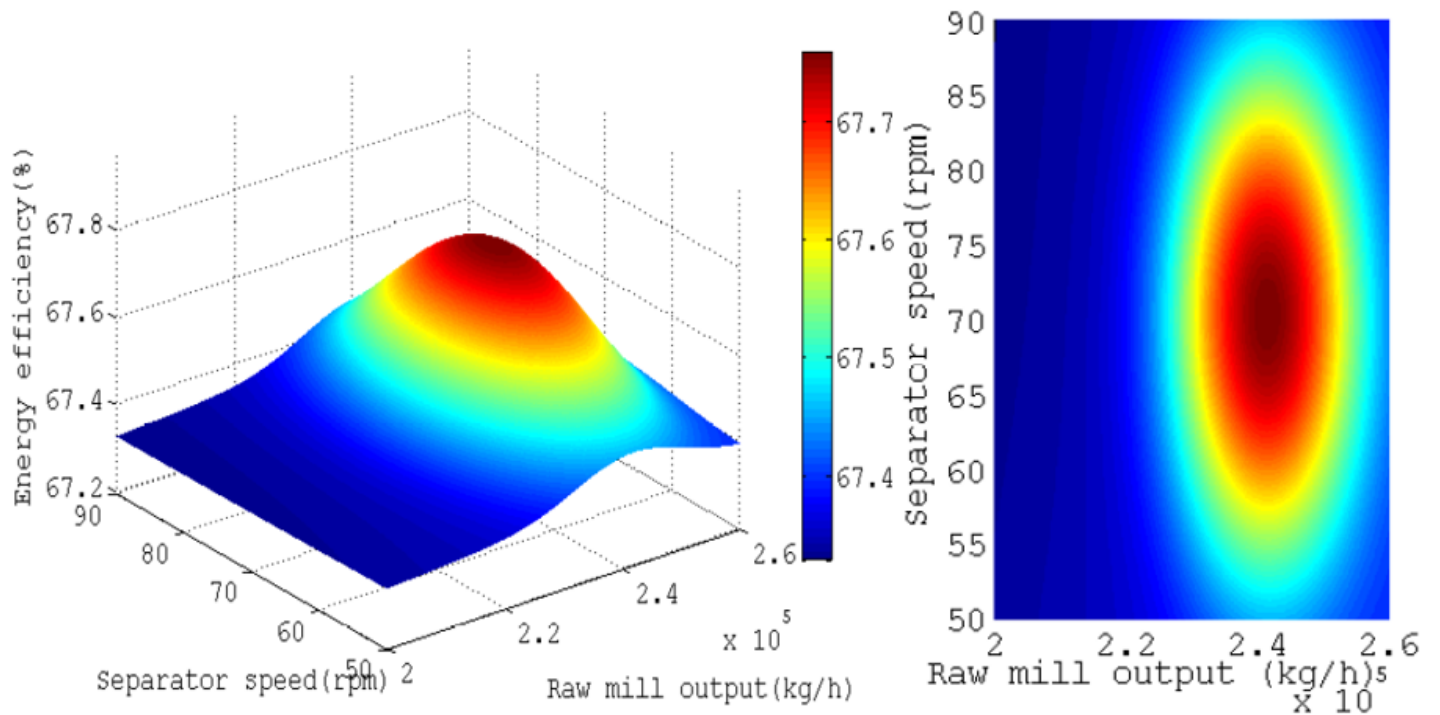


Figure 10

Comparison of predicted and measured energy efficiency values for PSO-ANFIS-GP10





**Figure 11**

Interaction between the raw mill output and mill separator speed (surface and contour plot)

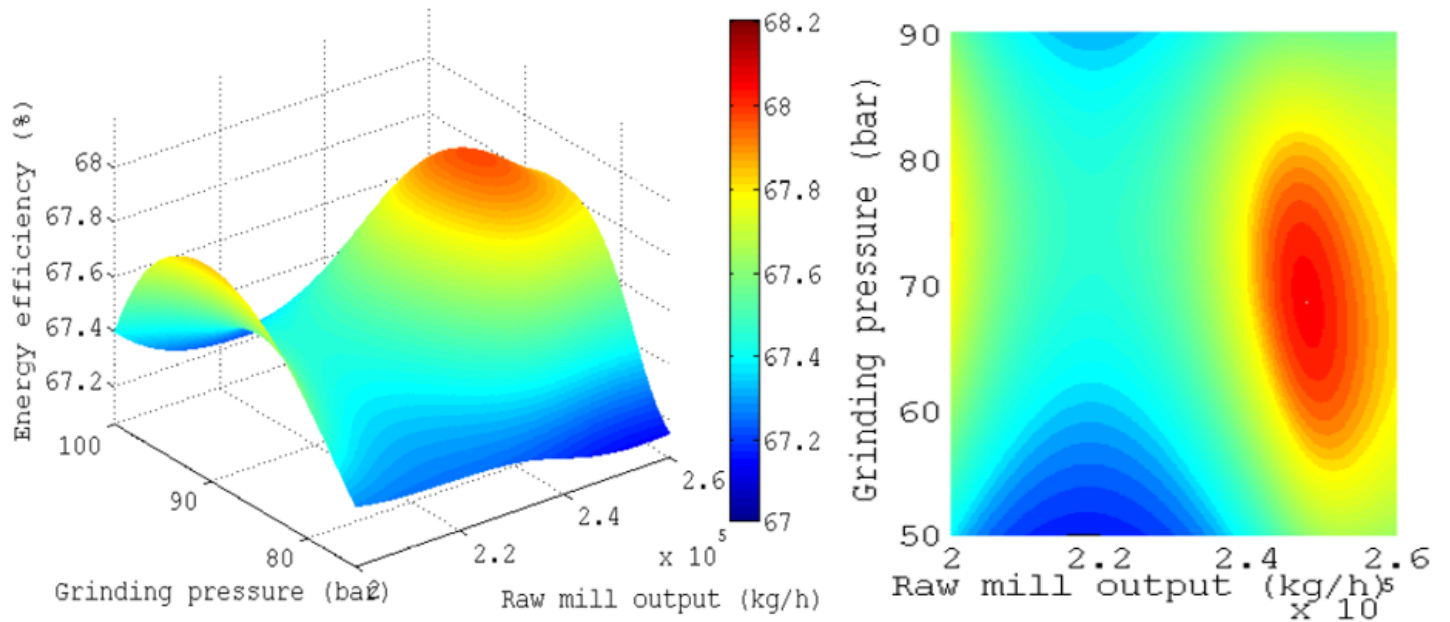


**Figure 12**

Interaction between the raw mill output and grinding pressure (surface and contour plot)

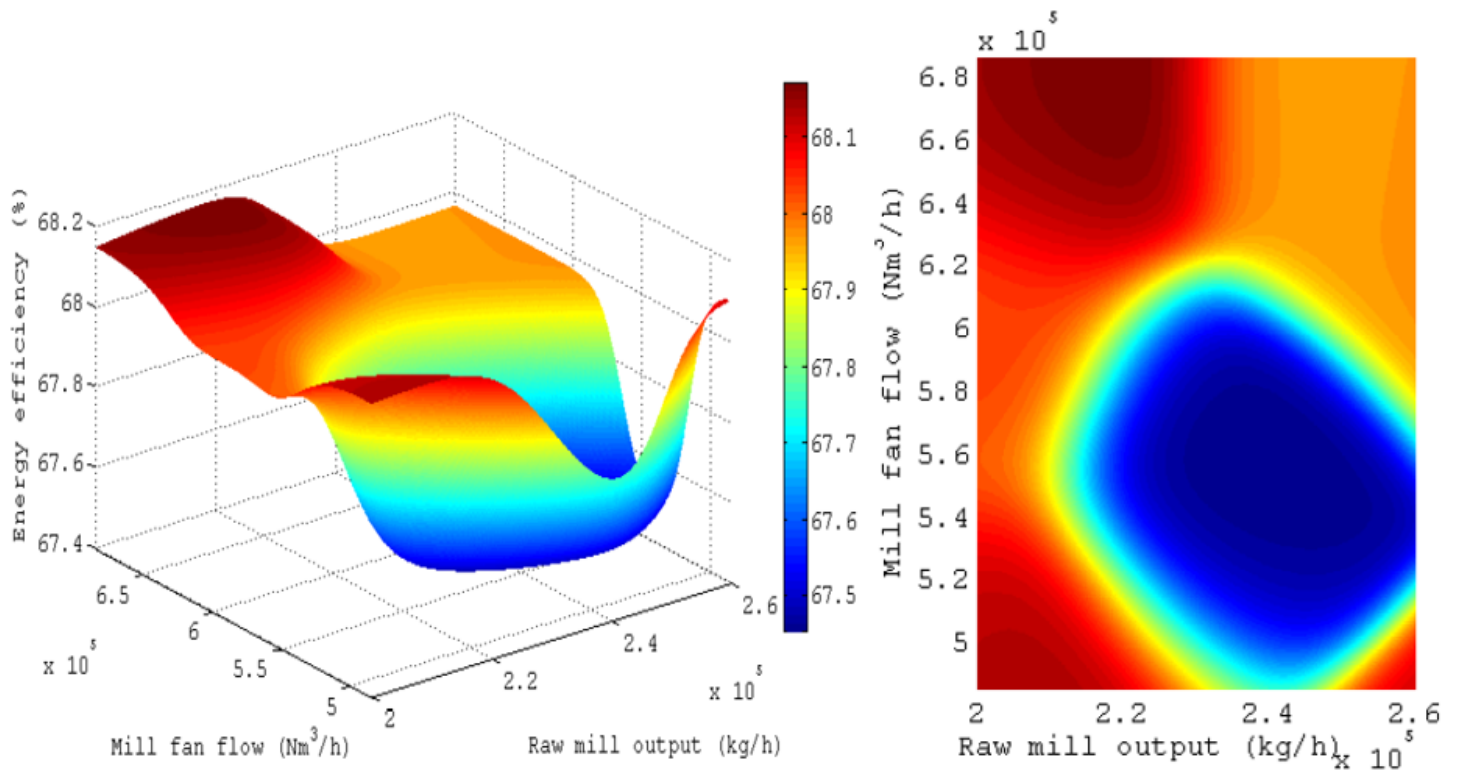


**Figure 13**

Interaction between the raw mill output and mill fan flow (surface and contour plot)

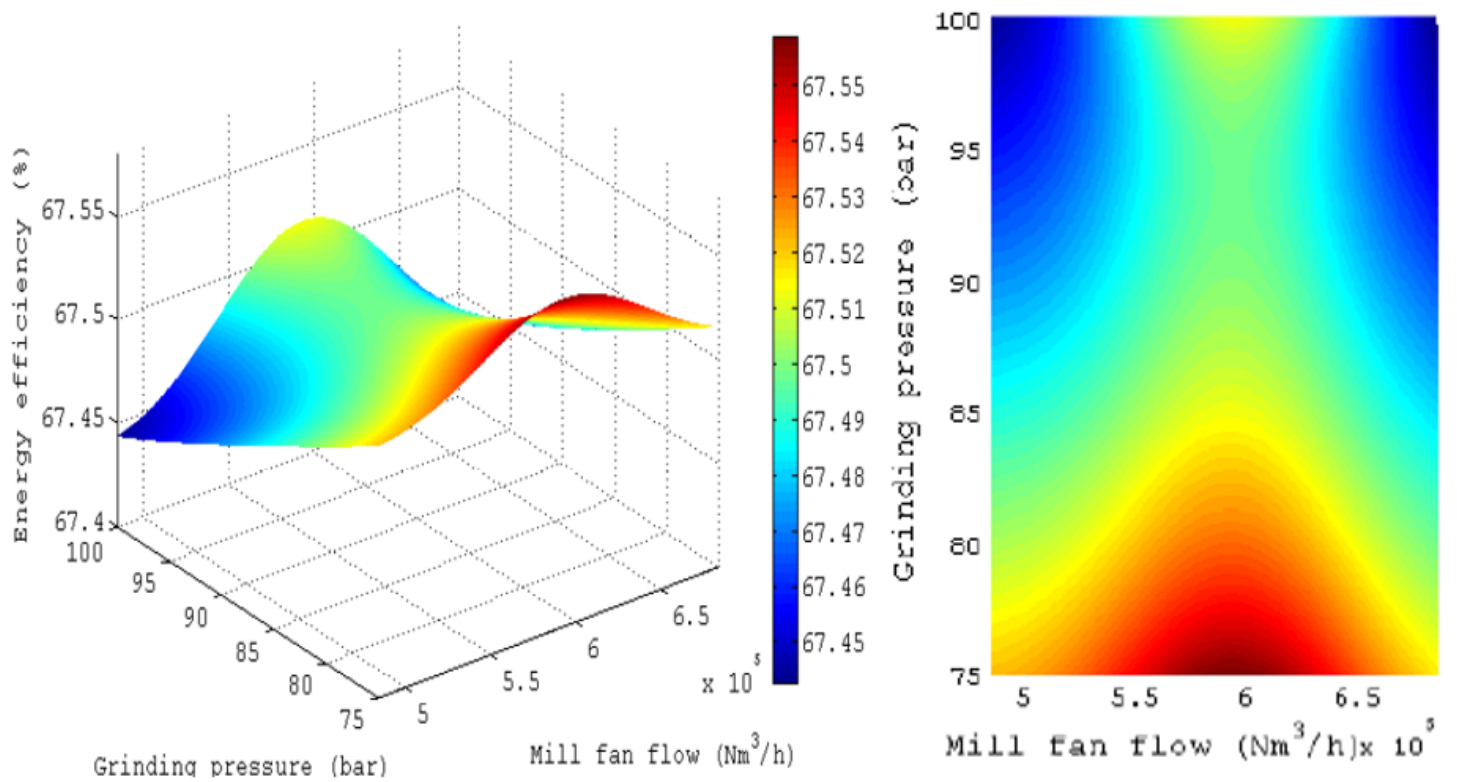


**Figure 14**

Interaction between the mill fan flow and grinding pressure (surface and contour plot)

## Supplementary Files

This is a list of supplementary files associated with this preprint. Click to download.

- [Supplementarydata.docx](#)